Molecular Diversity
https://doi.org/10.1007/s11030-024-10920-x

ORIGINAL ARTICLE

Discovery of a novel pyrido[1,2-*a*]thiazolo[5,4-*d*]pyrimidinone derivatives with excellent potency against acetylcholinesterase

Yan Zeng[1,3] · Zhifeng Chen[1] · Zhiyong Yang[1] · Fangxue Yuan[1] · Lifei Nie[2] · Chao Niu[2,3]

Received: 18 April 2024 / Accepted: 17 June 2024

Abstract

As mimetic compounds of the natural alkaloid mackinazolinone, forty pyrido[1,2-*a*]thiazolo[5,4-*d*] pyrimidinone were designed and synthesized from a bioisosterism approach. The structure of these compounds was confirmed through analysis using ^{1}H NMR, ^{13}C NMR, and HRMS techniques. All the compounds were evaluated for their anticholinesterase activities and cytotoxicity on normal cells (293 T) by the Ellman method and methyl thiazolyl tetrazolium (MTT) method in vitro. and the structure–activity relationships (SARs) were summarized. The results showed that most of the compounds effectively inhibited acetylcholinesterase (AChE) in the micromolar range with weak cytotoxicity. Compound 7o exhibited the best inhibitory activity against AChE, displaying an IC_{50} values of 1.67 ± 0.09 μM and an inhibitory constant K_i of 11.31 μM as a competitive inhibitor to AChE. Molecular docking indicated that compound 7o may bind to AChE via hydrogen bond and π–π stacking. Further molecular dynamics (MD) simulations indicated a relatively low binding free energy (− 27.91 kJ·mol^{-1}) of compound 7o with AChE. In summary, the collective findings suggested that 7o was promising as a potential novel drug candidate worthy of further investigation for the treatment of Alzheimer's disease.

Keywords Thiazolo[5,4-*d*]pyrimidinone · Bioisosterism · Acetylcholinesterase · Molecular docking · Molecular dynamics

Introduction

Alzheimer's disease (AD), the most common form of dementia, is a chronic and neurodegenerative illness with a number of symptoms, including loss of memory, deterioration in the use of language, mood swings, and loss of bodily functions [1–4]. Although many factors have been implicated in AD, its etiology is not completely clear. There are diverse pathologic factors responsible for AD, such as deficits of acetylcholine (ACh), *β*-amyloid peptide (A*β*) deposits, tau protein (*τ*) aggregation, neuroinflammation, and oxidative stress [5–10]. Among the diverse pathologic factors, ACh plays a significant role in the disease. The observation of a deficiency in cholinergic neurotransmission in AD has led to the cholinergic hypothesis as a classical theory in AD pathology proposed in 1976 [11], which states that the neurotransmitter ACh in the hippocampus and the neocortex regions plays a key role in learning and memory [12], and the remarkable decline in the level of ACh is primarily responsible for the dementia of AD patients. Under physiological conditions, acetylcholinesterase (AChE) can hydrolyze ACh to choline and acetate with a high efficiency [13]. Thus, inhibition against AChE is an advisable way to enhance the concentration of ACh in the synaptic cleft, rendering it a crucial target in the cholinergic system. Current treatment of AD with AChE inhibitors (tacrine, donepezil, galantamine and rivastigmine Fig. 1) could only improve symptoms but not address AD's etiology. Therefore, much effort has been made to develop more effective drug for the treatment of AD [14].

✉ Lifei Nie
nielf@ms.xjb.ac.cn

✉ Chao Niu
niuchao@ms.xjb.ac.cn

[1] Xinjiang Key Laboratory of Coal Mine Disaster Intelligent Prevention and Emergency Response, Xinjiang Institute of Engineering, Urumqi 830023, China

[2] State Key Laboratory Basis of Xinjiang Indigenous Medicinal Plants Resource Utilization, CAS Key Laboratory of Chemistry of Plant Resources in Arid Regions, Xinjiang Technical Institute of Physics and Chemistry, Chinese Academy of Sciences, Urumqi 830011, China

[3] University of Chinese Academy of Sciences, Beijing 100049, China

Published online: 27 June 2024

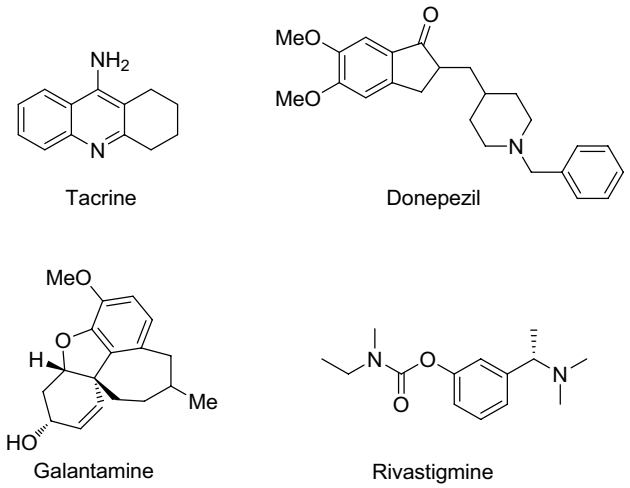

Fig. 1 Structures of ChE inhibitors used for the management of AD

Natural products have historically provided medicinal chemists with an important source of bioactive scaffolds for the development of new drug candidates [15–21]. Quinazolinone alkaloids are commonly found in natural products and pharmaceuticals that display biological activities in diverse areas, including cancer, CNS systems, inflammation, and hypertension [22, 23]. Among them, pyrido[2,1-*b*] quinazolinone alkaloids such as mackinazolinone, possesses a broad spectrum of pharmacological activities [24]. In recent years, some mackinazolinone derivatives have been found to improve cognitive dysfunction in an AD mouse model in vivo [25]. Inspired by the similarity of tricyclic scaffold of the mackinazolinone and tacrine, a scaffold hopping strategy was applied to synthesize pyrido[1,2-*a*] thiazolo[5,4-*d*]pyrimidinone, in which the benzene was substituted by thiazole (Fig. 2A). As a matter of fact, preliminary molecular docking indicated that both mackinazolinone and tacrine could be inserted vertically into the pocket of AChE (PDB: 4EY7) and interact with the residues around the binding site. However, the pocket exhibits a narrow and elongated structure resembling a ''boot'', and due to their limited length, these two compounds are insufficient to establish additional favorable interactions between ligands and proteins (Fig. 2B). Thus, in this study, a lipophilic R group is introduced to the thiazole moiety, and forty pyrido[1,2-*a*]thiazolo[5,4-*d*] pyrimidinone compounds were prepared. Their inhibitory activity on AChE and BChE and the cytotoxicity on normal cells were evaluated in vitro.

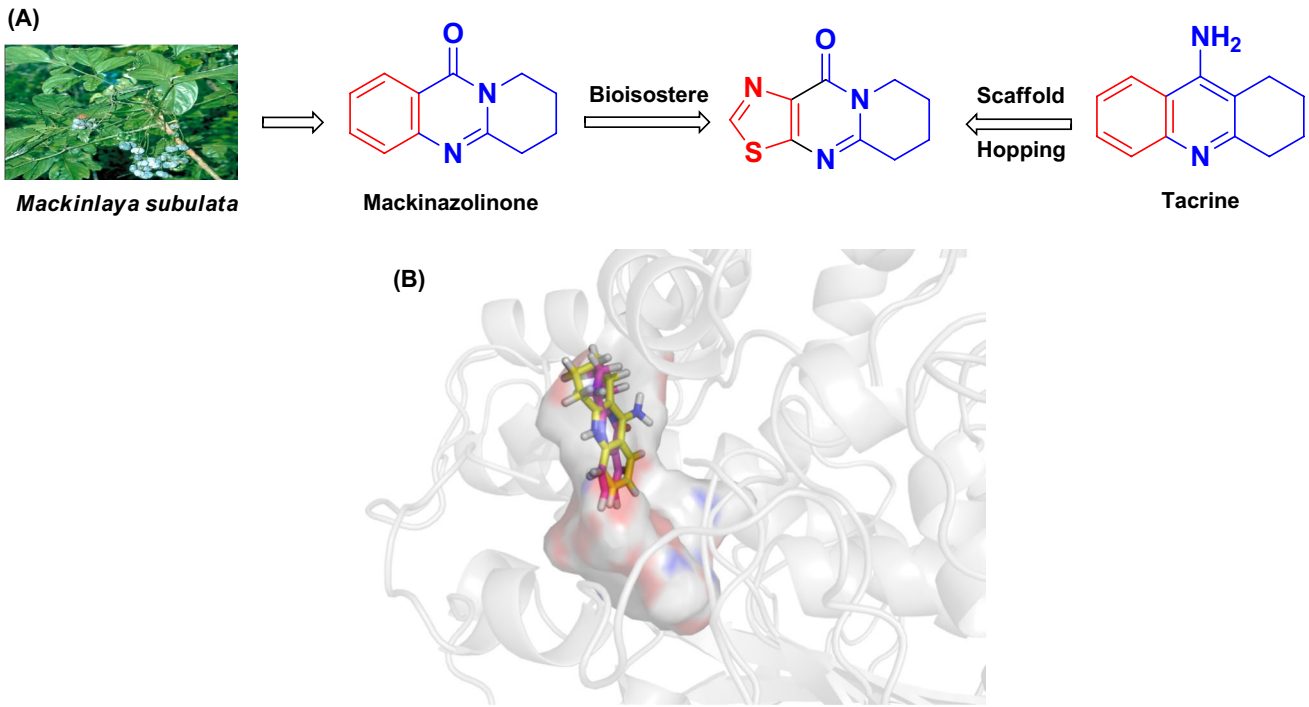

Fig. 2 **A** Design rational of target compounds via scaffold hopping strategy. **B** The 3D diagrams illustrating the docking mode of mackinazolinone and tacrine with human AChE (PDB: 4EY7). (The structure of AChE in complex with mackinazolinone and tacrine are depicted in ribbon-colored gray; mackinazolinone and tacrine are depicted in stick-colored magenta and yellow; the binding pocket was showed on the surface)

Results and discussion

Synthesis of compounds

The target compounds were prepared via a seven-step reaction as outlined in Scheme 1. Firstly, ethyl 2-cyano-2-(hydroxyimino)acetate 1 was prepared from the ethyl cyanoacetate in the sodium nitrite solution and 85% orthophosphoric acid conditions. Reduction of this oxime compound to amine 2 was performed using $Na_2S_2O_4$ in a $NaHCO_3$ solution [26]. The intermediates 3 were obtained with acetic anhydride in formic acid. Subsequently, compound 3 was treated with Lawesson reagent in toluene at 110 °C to acquire compound 4, which was converted to intermediates 5 with piperidine-2-one in the presence of phosphorus oxychloride. The intermediate 5 was brominated with NBS to yield the desired 2-bromo-7,8-dihydro-5*H*-pyrido[1,2-*a*]thiazolo[5,4-*d*]pyramidine-10(6*H*)-one 6 in good to high yield, which was coupled with the various substituted phenylboronic acid through the Suzuki coupling reaction to acquire target compounds 7a-7an.

The optimized reaction conditions for the Suzuki coupling reaction were 1 mmol of 6, 0.05 mmol of $Pd(PPh_3)_4$, 3 mmol of K_2CO_3, 8 mL of toluene/water = 3:1, 110 °C, 24 h). Under these conditions, the target compounds 7a-7an were synthesized efficiently in high yields. The structures of all synthetic derivatives were elucidated by ^{1}H-NMR, ^{13}C-NMR and HRMS data, as described in the experimental section. The single crystal of 7am was obtained in EtOH (Fig. 3), which is consistent with the structural formula described in Scheme 1. The spectroscopic data and analysis of synthetic derivatives could be found in supporting information.

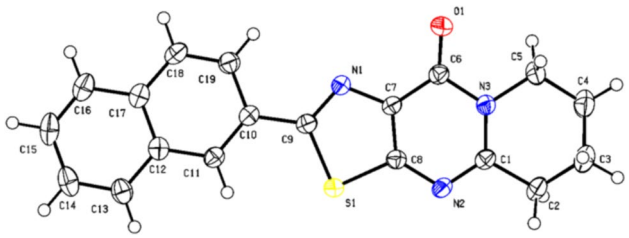

Fig. 3 Crystal structure of compound 7am (CCDC: 2,105,974)

AChE and BChE inhibitory activity of 7a-7an

The inhibitory activity of the synthesized compounds was evaluated against electric eel-derived AChE (eeAChE) and equine serum-derived BChE (eqBChE) using the spectrophotometric method described by Ellman [27]. All compounds at the initial concentration of eeAChE at 10 μM and eqBChE at 100 μM were screened to select those with inhibitory potency higher than 50%, for which the IC_{50} values were determined. Tacrine and huperzine A were used as reference compounds in the assay. The results of the biological evaluation were presented in Table 1

In terms of the structure–activity relationship, the majority of the tested compounds exhibited a notable level of anti-AChE activity, surpassing their anti-butyrylcholinesterase (BChE) activity within the micromolar range. Obviously, these compound exhibited higher selectivity to AChE than BChE. Compared with aromatic compounds, heterocyclic

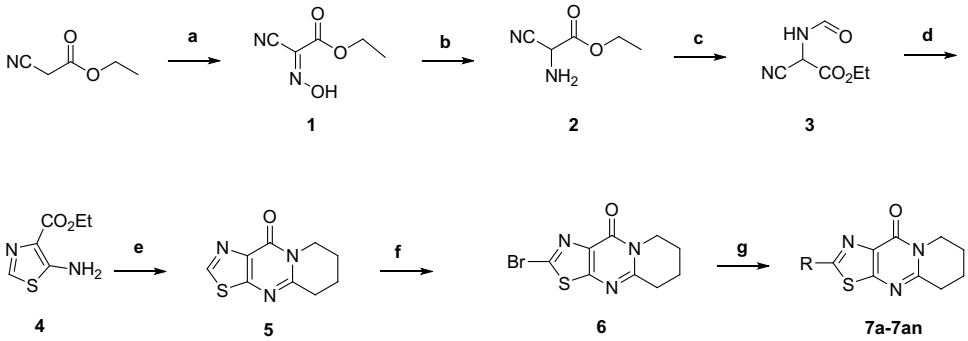

Scheme 1 Synthetic route for the target compounds. *Reagents and conditions*: **a** $NaNO_2$, H_3PO_4, HCl, 0–45 °C; **b** $NaHCO_3$, $Na_2S_2O_4$, 35 °C, 2 h.; **c** HCOOH, $(Ac)_2O$, reflux, 8 h.; **d** $PhCH_3$, Lawesson reagent, reflux, 12 h.; **e** $POCl_3$, piperidin-2-one, DCM, reflux, 12 h.; **f** NBS, acetonitrile.; **g** $Pd(PPh_3)_4$, K_2CO_3, $PhCH_3$/H_2O = 3:1, reflux, 24 h

7a R= Ph-
7b R= 2-CH_3Ph-
7c R= 3-CH_3Ph-
7d R= 4-CH_3Ph-
7e R= 4-$C(CH_3)_3$Ph-
7f R= 2-ClPh-
7g R= 3-ClPh-
7h R= 4-ClPh-
7i R= 2-BrPh-
7j R= 3-BrPh-
7k R= 4-BrPh-
7l R= 2-FPh-
7m R= 4-FPh-
7n R= 2-CF_3Ph-
7o R= 4-CF_3Ph-
7p R= 3-OCH_3Ph-
7q R= 4-OCH_3Ph-
7r R= 2-CNPh-
7s R= 3-CNPh-
7t R= 4-CNPh-
7u R= 4-CHOPh-
7v R= 3-CH_3COPh-
7w R= 3-NO_2Ph-
7x R= 3,5-diCH_3Ph-
7y R= 3,5-diClPh-
7z R= 3,4-diClPh-
7aa R= 3,5-diBrPh-
7ab R= 3,5-diFPh-
7ac R= 3,5-diOCH_3Ph-
7ad R= 3,4-diOCH_3Ph-
7ae R= 3-Cl-4-FPh-
7af R= furan-3-
7ag R= benzofuran-2-
7ah R= thiophen-3-
7ai R= benzothiophene-2-
7aj R= 1,1'-biphenyl-2-
7ak R= 1,1'-biphenyl-4-
7al R= oxydibenzenyl-4-
7am R= naphth-2-
7an R= dibenzo[*b*,*d*]furan-4-

Table 1 Median inhibition concentration of compound 7a-7an Cell lines (IC_{50}, μM)

No	R	IC_{50}[c], μM or IR[d], %		SI[e]	293 T
		eeAChE[a]	eqBChE[b]		
7a	R = Ph-	9.12 ± 0.24	< 30%	–	> 50
7b	R = 2-CH_3Ph-	37.09%	< 30%	–	> 50
7c	R = 3-CH_3Ph-	7.56 ± 0.40	< 30%	–	> 50
7d	R = 4-CH_3Ph-	10.44 ± 0.31	< 30%	–	> 50
7e	R = 4-$C(CH_3)_3$Ph-	5.53 ± 0.13	< 30%	–	> 50
7f	R = 2-ClPh-	10.16 ± 0.17	< 30%	–	> 50
7 g	R = 3-ClPh-	6.97 ± 0.32	40.50%	–	> 50
7 h	R = 4-ClPh-	8.26 ± 0.22	32.53%	–	> 50
7i	R = 2-BrPh-	32.92%	< 30%	–	> 50
7j	R = 3-BrPh-	6.48 ± 0.15	31.5%	–	> 50
7 k	R = 4-BrPh-	2.49 ± 0.27	32.12 ± 0.94	12.90	> 50
7 l	R = 2-FPh-	36.29%	< 30%	–	> 50
7 m	R = 4-FPh-	5.46 ± 0.07	35.76%	–	> 50
7n	R = 2-CF_3Ph-	< 30%	< 30%	–	> 50
7o	R = 4-CF_3Ph-	1.67 ± 0.09	51.43 ± 1.30	30.79	> 50
7p	R = 3-OCH_3Ph-	6.19 ± 0.01	< 30%	–	> 50
7q	R = 4-OCH_3Ph-	3.39 ± 0.23	43.31%	–	> 50
7r	R = 2-CNPh-	< 30%	< 30%	–	> 50
7 s	R = 3-CNPh-	2.94 ± 0.07	41.26 ± 0.92	14.03	> 50
7t	R = 4-CNPh-	4.33 ± 0.27	< 30%	–	> 50
7u	R = 4-CHOPh-	6.87 ± 0.38	< 30%	–	> 50
7v	R = 3-CH_3COPh-	2.46 ± 0.06	< 30%	–	> 50
7w	R = 3-NO_2Ph-	3.11 ± 0.26	< 30%	–	> 50
7x	R = 3,5-diCH_3Ph-	39.36%	< 30%	–	> 50
7y	R = 3,5-diClPh-	9.31 ± 014	< 30%	–	> 50
7z	R = 3,4-diClPh-	5.83 ± 0.36	< 30%	–	> 50
7aa	R = 3,5-diBrPh-	5.35 ± 0.61	< 30%	–	> 50
7ab	R = 3,5-diFPh-	3.35 ± 0.10	49.0%	–	> 50
7ac	R = 3,5-diCH_3OPh-	8.58 ± 0.32	< 30%	–	> 50
7ad	R = 3,4-diCH_3OPh-	7.01 ± 0.25	< 30%	–	> 50
7ae	R = 3-Cl-4-FPh-	9.18 ± 0.30	< 30%	–	> 50
7af	R = furan-3-	34.91%	< 30%	–	> 50
7ag	R = benzofuran-2-	44.61%	< 30%	–	> 50
7ah	R = thiophen-3-	47.19%	< 30%	–	> 50
7ai	R = benzo thiophen-2-	36.29%	< 30%	–	> 50
7aj	R = 1,1'-biphenyl-2-	35.50%	< 30%	–	> 50
7ak	R = 1,1'-biphenyl-4-	< 30%	< 30%	–	> 50
7al	R = oxydibenzenyl-4-	4.96 ± 0.39	41.19%	–	> 50
7am	R = naphth-3-	48.50%	< 30%	–	> 50
7an	R = dibenzo[b,d]furan-4-	< 30%	< 30%	–	> 50
Tacrine		0.037 ± 0.001	5.24 ± 0.02	–	–
Huperzine A		0.25 ± 0.01	–	–	–

[a]AChE (E.C. 3.1.1.7) from electric eel

[b]BChE (E.C. 3.1.1.8) from horse serum

[c]Concentration required for 50% inhibition of ChEs, data were shown in mean ± SD of triplicate independent experiments

[d]Inhibitory rate of the compounds under 10 μM on eeAChE and 100 μM on eqBChE

[e]Selectivity index (SI) = BChE IC_{50}/AChE IC_{50}

[f]Not determined

aromatic (7af-7an) were almost inactive to anti-AChE activity except for 7al. These results might indicate that those substitution groups were unfavorable for anti-AChE activity.

It could be concluded that the variation of the substituent groups on the benzene ring affects the enzyme inhibitory potency. The electron-donating $–CH_3$–OCH_3–$diCH_3$ and $–diOCH_3$ substituents on the phenyl ring showing significant inhibition against AChE. The order of activity was $–OCH_3$ > $–diOCH_3$ > $–CH_3$ > $–diCH_3$. With the electron-withdrawing groups (halogens, trifluoromethyl and cyano atom), it has displayed excellent inhibitory potential for AChE. For compounds with F, the order of activity was 3,5-diF > 4-F > 2-F, the order of activity observed for Cl was 3,4-diCl_2 > 3-Cl > 4-Cl > 3,5-diCl > 2-Cl, And the order was 4-Br > 3,5-diBr > 3-Br > 2-Br for Br atom, the order of activity observed for CF_3 groups was 4-CF_3 > 2-CF_3, and the order was 3-CN > 4-CN > 2-CN for CN groups. Obviously, the variation of substituent groups ($–NO_2$, –CHO, CH_3CO–) on benzene ring significantly affect the potency as well. It was worth noting that compound 7o with 4-trifluoromethyl substitution (IC_{50} = 1.67 ± 0.09 µM) exhibited the most potent AChE inhibitory activity. Next, we explored the impact of the substituent position on the benzene ring on AChEs inhibitory activities; the activity for AChE was *para-* and *meta-* > *ortho-*.

Kinetic studies of AChE inhibition

In order to determine the kinetic type of AChE inhibition, a kinetic study was performed on 7o, the most active AChE inhibitor. The rate of AChE effect was measured at three different concentrations of 7o using different concentrations of the substrate acetylthiocholine (Fig. 4). In every case, the initial velocity was measured at different concentrations of the acetylthiocholine, and the reciprocal of the initial velocity (1/v) was plotted against the reciprocal of [acetylthiocholine]. Lineweaver–Burk plots for 7o displayed that the plots of 1/V versus 1/[S] gave straight lines with different slopes depending on concentrations of the inhibitor, and the lines intersected on the vertical axis. The V_{max} value is unchanged regardless of the concentration of the inhibitor, and K_m increases with increasing concentration of the inhibitor. This behavior indicates that 7o inhibits the AChEs competitively. In addition, a secondary plots was constructed to calculate the steady-state inhibition constant (which gave K_i values of 11.31 µM against AChE) of 7o [28].

Docking studies

To investigate the binding mode of the 7o with AChE (PDB:4EY7) [29], our docking simulation of 7o with AChE was performed using the AutoDock [30]. As shown in Fig. 5, the 7o displayed a nearly identical configuration as Donepezil did, when bound to the gorge site of human AChE. The hydrogen bonding and π–π stacking were two major interactions between the ligands and the AChE. In brief, the 7o formed a hydrogen bond with Phe295 as Donepezil did, its carbonyl and the Phe residue. The complex was further stabilized by π–π stacking of the ligand's thiazole and pyrimidine ring with the benzene ring of the Tyr341. Lastly, the binding was also promoted by favorable van der Waals (dispersive) interactions. All of the above led to a better inhibitory activity against AChE, which was consistent with our previous results.

Molecular dynamics

By integrating Newton's classical equation of motion, MD simulations typically compute atom movements over time.

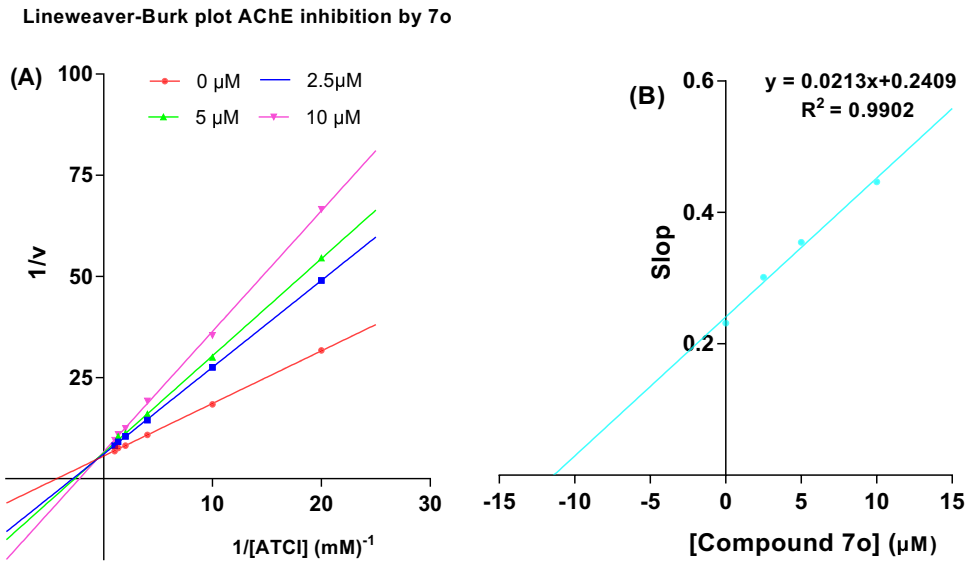

Fig. 4 Mechanism of AChE inhibition by compounds 7o (**A**) to AChE, and their K_i determination (**B**)

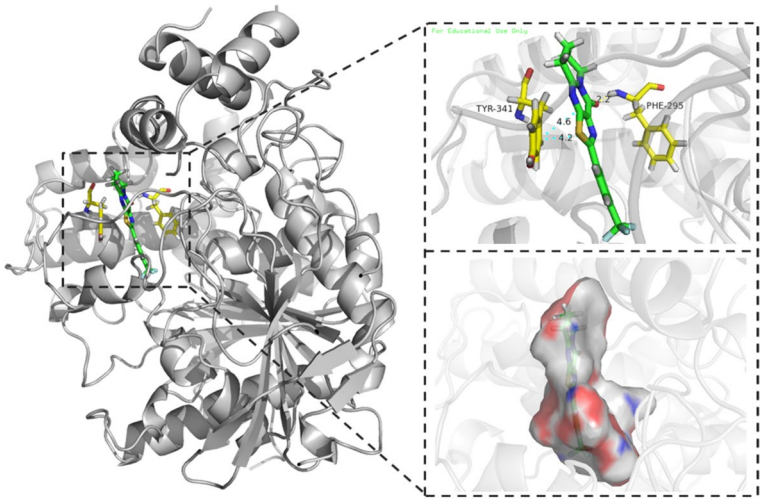

Fig. 5 The 3D diagrams illustrating the docking mode and interaction of 7o with human AChE (PDB: 4EY7). (The structure of AChE in complex with 7o was depicted in ribbon colored gray; Compound 7o and residue Phe295, Tyr341 was depicted in stick colored green and yellow; The binding pocket was showed in surface)

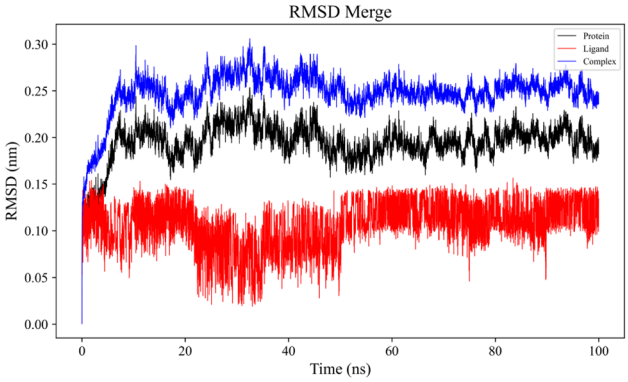

Fig. 6 RMSD plot of 7o–4EY7 complex (blue), 4EY7 apo (black), 7o (red) across 100 ns MD simulation trajectory

Simulations were used to predict the ligand binding status in the physiological environment [31, 32]. The docked complexes of **7o** with microtubule protein (PDB: 4EY7) in docking experiments were considered as the initial structures for the MD run. The software Gromacs was used to model molecular dynamics for 100 ns.

Root mean square deviation (RMSD)

The MD trajectory was used to calculate the residual flexibility of the protein backbone (C-alpha). The mean change in RMSD of the protein–ligand complex is acceptable within 1–3 Å. The RMSD plots for native protein, ligand (7o) and protein–ligand complex were shown in Fig. 6. The RMSD value for the 7o–4EY7 complex varied from 0.87 Å to 3.06 Å (Table 2). It reached equilibrium at 50 ns, according to the plot. Following that, fluctuations in RMSD values remained within 1.0 Å for the duration of the simulation, which was perfectly fine. The ligand 7o showed a minor deviation between 20–50 ns in the binding site, but later on a consistent behavior was noticed. The small fluctuation and low RMSD values indicated the conformations of protein backbones were stable relative to their initial structures.

Table 2 The minimum, maximum and average values of different parameters, RMSD, RMSF, Rg,hydrogen bonding and binding free energy of 7o–4EY7 complex

	7o-4EY7 complex
Root-mean-square deviation (RMSD) Å	
Minimum	0.87
Maximum	3.06
Average	2.48
Root-mean-square fluctuation (RMSF) Å	
Minimum	0.41
Maximum	6.81
Average	1.19
Radius of gyration (Rg) Å	
Minimum	22.78
Maximum	23.61
Average	23.29

Root mean square fluctuation (RMSF)

RMSF can analyze the fluctuations of each amino acid in the protein. The higher peaks were related to loops, terminal ends and twist regions, since these regions oscillate more than any other part of the protein. At the same time, a lower value always occurred among residues around the binding site. The RMSF values of the protein-coupled to 7o are depicted in Fig. 7. The average value of fluctuation of residues ranged from 0.41 to 6.81 Å for the chain of 4EY7 (Table 2). The amino acid range Glu4–Glu7, Asp74–Asn87, Pro259–Asp266, Pro492–Ala497, and Asn533–Ala542 in

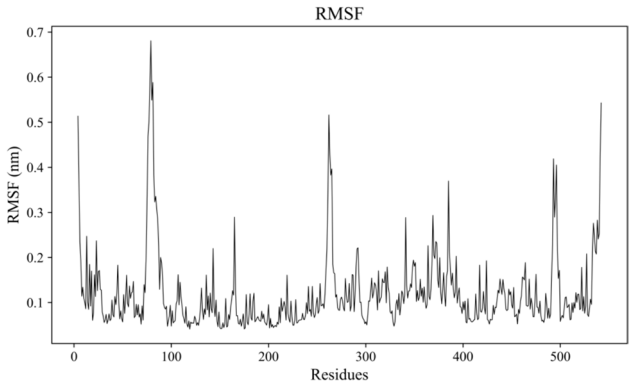

Fig. 7 RMSF plot of protein 4EY7 across 100 ns MD simulation trajectory

protein, which constituted loops and twists, had the biggest fluctuation during the simulation.

Radius of gyration (Rg)

The folding and unfolding of a complex during simulation can be determined using Rg, which implies the compactness when the secondary structure is packed in tertiary form. The lower the value of Rg more folded the structure. During the simulation, the 7o–4EY7 complex at around 20 to 60 ns appeared to undergo apparent conformational changes, which was consistent with RMSD and RMDF fluctuation (Fig. 8). After that, it declined and remained almost stable with an average of 23.29 Å (Table 2).

Hydrogen bonds analysis

The hydrogen bond was one of the most important interactions that was able to stabilize the protein–ligand complex system. As a result, interactions of hydrogen bonds between ligands (7o) and protein (4EY7) were examined throughout 100 ns of MD simulations (Fig. 9). The 7o–4EY7 complex formed more hydrogen bonds after 48 ns, and three hydrogen bonds were observed at most. The hydrogen bonds in the complex remained intact throughout the dynamics, suggesting greater interaction between compound 7o with microtubule protein (4EY7) and a stable conformation.

Binding free energy calculation

The total binding free energy of the corresponding complex (ΔGbind) was calculated by MM/PBSA methodology to evaluate binding affinities between compound 7o and AchE (4EY7), which included van der Waal energy, electrostatic energy, polar/nonpolar solvation energy, etc. These energies were expressed in kJ·mol^{-1}, and a more negative value represented a stronger binding achieved. The result revealed that the 7o–4EY7 complex had a rather low binding free energy (− 27.91 kJ·mol^{-1}) and thus exhibited a superior binding affinity towards AchE. Further, the Van der Waals energy (− 38.71 kJ·mol^{-1}) and electrostatic energy (− 9.90 kJ·mol^{-1}) constituted most of the binding free energy in the complex, among which the van der Waals energy contributed most. As shown in Fig. 10, the Tyr72 (ΔEvdw = − 1.408 kJ·mol^{-1}, ΔEele = − 0.582 kJ·mol^{-1}), ASP:74(ΔEvdw = − 0.749 kJ·mol^{-1}, ΔEele = − 0.314 kJ·mol^{-1}), Tyr124 (ΔEvdw = − 1.511 kJ·mol^{-1}, ΔEele = − 1.599 kJ·mol^{-1}), Trp286 (ΔEvdw = − 2.666 kJ·mol^{-1}, ΔEele = − 0.916 kJ·mol^{-1}), Val:294(ΔEvdw = −0.127 kJ·mo

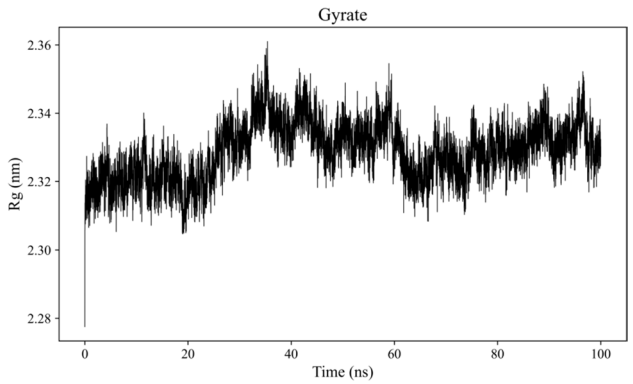

Fig. 8 Radius of gyration plot of 7o–4EY7 complex across 100 ns MD simulation trajectory

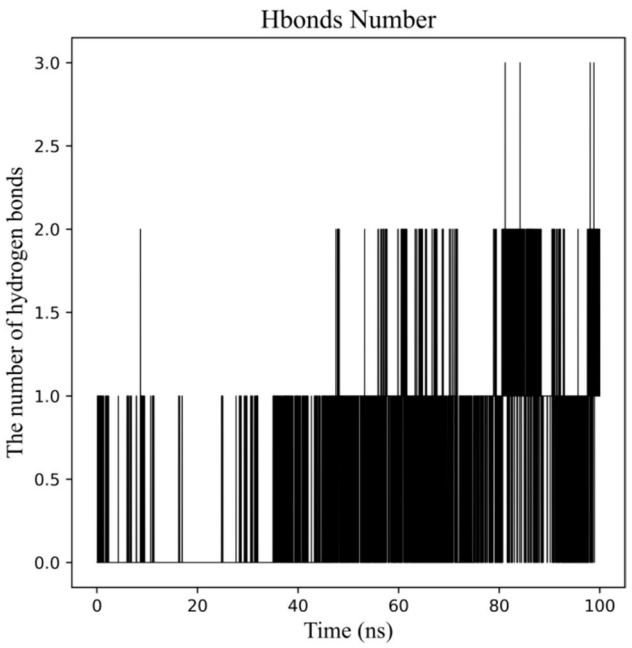

Fig. 9 Number of H-bonds in 7o–4EY7 complex across 100 ns MD simulation trajectory

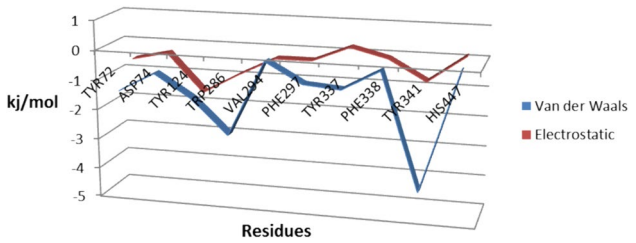

Fig. 10 Total energy decomposition of 7o–4EY7 complex across 100 ns MD simulation trajectory

l^{-1}, ΔEele = − 0.304 kJ·mol^{-1}), Phe:297(ΔEvdw = − 0.809 kJ·mol^{-1}, ΔEele = − 0.299 kJ·mol^{-1}), Tyr:337(ΔEvdw = − 0.910 kJ·mol^{-1}, ΔEele = − 0.208 kJ·mol^{-1}), Phe:338(ΔEvdw = − 0.223 kJ·mol^{-1}, ΔEele = − 0.096 kJ·mol^{-1}), Tyr341 (ΔEvdw = − 4.094 kJ·mol^{-1}, ΔEele = − 0.780 kJ·mol^{-1}), His :447(ΔEvdw = − 0.062 kJ·mol^{-1}, ΔEele = − 0.113 kJ·mol^{-1}) may be more important than other residues for the protein–ligand interaction, since a lower Van der Waals and electrostatic energies were found for them by energy decomposition.

The folding free-energy landscape (FEL) characterizes the free energy changes of proteins during the simulation. The FEL is generally plotted by two quantities that describe the characteristics of the system, such as principal components PC1 and PC2, as shown in Fig. 11, the complex had a FEL depicting one minimum free-energy basins, which appeared at 99 ns during the simulation. The conformation was also extracted and analyzed from the minimum free-energy basin. The compound 7o could form four hydrogen bonds with Trp86, Tyr337 in protein 4EY7, which was in agreement with the hydrogen bonds analysis in Fig. 9.

Cell toxicity studies

In order to gain an understanding of the potential harmful effects of the target compounds, an assessment was conducted to determine their cytotoxicity on normal cell line (293T) through the utilization of the MTT assay method [33]. The results in Table 1 showed that all compound were nearly non-toxic to 293 cells, which possesses great safety for the development of these compounds as new AChE inhibitors.

Conclusion

In summary, in the present studies, we describe the synthesis and biological evaluation of 40 new tricyclicthiazolo[5,4-*d*] pyrimidinone. These compounds are moderately potent and selective AChE inhibitors, with no activity toward BChE. Compound 7o exhibited the most potent inhibitory activity against AChE with an IC_{50} values of 1.67 ± 0.09 μM.

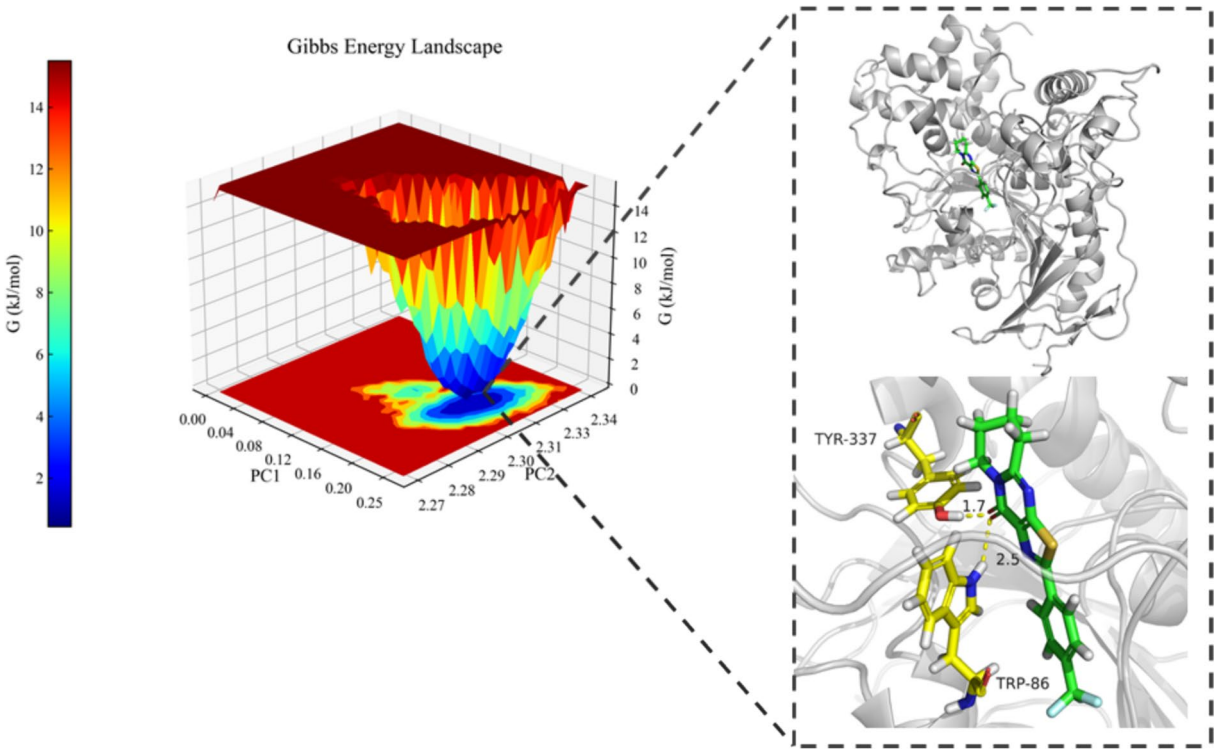

Fig. 11 FEL of 7o–4EY7 complex along PC1 and PC2. (The conformations extracted from the minimum free-energy basins are next to FEL)

Compounds with IC_{50} less than 10 μM on AChE were further evaluated for cytotoxic activity on 293 cells. The inhibition kinetics of 7o was analyzed using Lineweaver–Burk plots, which revealed that the compound was a competitive-type inhibitor. The molecular docking results indicate that 7o was more likely to bind to the active center of AChE, which hindered the substrate acetylthiocholine iodide (ATCI) from binding to the enzyme, resulting in the decrease in enzyme activity, and that 7o may interact with AchE (4EY7) through hydrogen bonding and π–π stacking. Lastly, 100 ns MD simulations of hit in complex with AchE were conducted. The results of RMSD, RMSF and Rg show that the complexes had good stability. On this basis, the MM/PBSA methodology was employed to calculate binding free energy, and compound 7o had a superior affinity for binding with protein. In summary, these findings highlight the potential of 7o as a promising novel drug for the treatment of Alzheimer's disease.

Experimental section

General information

All the chemicals were purchased from commercial companies and used without purification. All reactions were monitored by analytical thin layer chromatography (TLC) on silica gel G60F-254 precoated plates (purchased from Qingdao Haiyang Inc, Qingdao, China). Visualization was achieved using UV light (254 and 365 nm), flash column chromatography was performed with silica gel (200–300 mesh) purchased from Qingdao Haiyang Chemical Co. Ltd. Melting points were determined using a Buchi B-540 melting point apparatus. Nuclear magnetic resonance (NMR) spectra are recorded on Varian 400 MHz and Bruker AVANCE NEO 600 MHz instruments in $CDCl_3$. Chemical shifts are reported in parts per million (d) downfield from the signal of tetramethylsilane (TMS) as the internal standard. Coupling constants are reported in Hz. All chemical shifts are reported in parts per million (ppm) relative to the internal standard. High-resolution mass spectra (HRMS) were measured with the AB SCIEX QSTAR Elite quadrupole time-of-flight mass spectrometry at 70 eV ionization energy. HPLC was performed on a Shimadzu LC-2030C 3D instrument (Shimadzu Corp., Japan) with UV detection, employing an Acclaim 120 C18 column (4.6 mm × 250 mm, 5 μm), Waters, MA, USA.

Experimental procedures

Ethyl 2-amino-2-cyanoacetate (2)

A solution of sodium nitrite (57.3 g, 0.83 mol) in water (650 mL) was treated with ethyl cyanoacetate (100 g, 0.83 mol), orthophosphoric acid (85%, 36.6 mL, 0.55 mol) was added dropwise while keeping the temperature of the reaction mixture below – 10 °C with the aid of an ice bath. At the end of the addition, the mixture was warmed to 40 °C and stirred for 1 h. After completion of the reaction (monitored by TLC, eluent petroleum ether: ethyl acetate = 5:1, $R_f = 0.28$), the reaction was quenched at 35 °C with fuming HCl (74 mL, 0.88 mol), and the mixture was then left to cool to room temperature and at 0 °C overnight to complete precipitation. The solid was filtered, the filtrate was washed with water and dried under a high vacuum overnight to white crystal 1.

To a stirred solution of 1 (20 g, 0.14 mol) in water (250 mL) was added a saturated solution of $NaHCO_3$ in water (160 mL), followed by the addition of $Na_2S_2O_4$ (73 g, 0.42 mol). The reaction mixture was warmed up to 35 °C and stirred for additional 2 h. After completion of the reaction (monitored by TLC, eluent petroleum ether: ethyl acetate = 2:1, $R_f = 0.52$), it was then saturated with NaCl (150 mL) and extracted with DCM (3 × 350 mL). Combined organic layers were washed with brine, dried over Na_2SO_4, filtered and concentrated *in vacuo* to give desired compound 2, Yield 27%, red oil liquid, ^{1}H NMR (400 MHz, $CDCl_3$) δ 4.45 (s, 1H), 4.34 (q, $J = 7.1$ Hz, 2H), 2.31 (s, 2H), 1.36 (t, $J = 7.2$ Hz, 3H).

Ethyl 5-aminothiazole-4-carboxylate(4)

A mixture of acetic anhydride (1.8 g, 18 mmol) and formic acid (0.83 g, 18 mmol) was heated to 55 °C for 2 h, The reaction mixture was then cooled 0 °C and a solution of ethyl-2-amino-2-cyanoacetate (1.28 g, 10 mmol) in THF (10 mL) was added dropwise. The mixture was allowed to warm to RT for 8 h. After completion of the reaction (monitored by TLC, eluent petroleum ether: ethyl acetate = 5:1, $R_f = 0.38$), it was then quenched with saturated NaCl (150 mL) and extracted with DCM (3 × 350 mL). Combined organic layers were washed with brine, dried over Na_2SO_4, filtered and concentrated *in vacuo* to give desired compound 3 as a light yellow solid that was used at the next step without additional purification [34].

To a solution of ethyl 2-cyano-2-formamidoacetate (1.56 g, 10 mmol) in anhydrous toluene (10 mL). Lawesson's reagent (2.0 g, 5 mmol) was added in one portion. The obtained yellow suspension was stirred overnight at reflux for 12 h under the N_2 atmosphere. After completion of the reaction (monitored by TLC, eluent petroleum ether: ethyl acetate = 10:1, $R_f = 0.47$), the reaction mixture was cooled to 0 °C and extracted with DCM (2 × 30 mL). The organic phase was washed with brine. The organic layer was separated and dried over anhydrous Na_2SO_4, filtered, and concentrated under reduced pressure to give the crude product, which was purified by silica gel chromatography

(petroleum ether/ethyl acetate = 5:1) to produce the pure corresponding compound 4 [35]. Yield 67%, light yellow solid, m p 135–136 °C; ^{1}H NMR (400 MHz, $CDCl_3$) δ 7.88 (s, 1H), 6.00 (s, 2H), 4.39 (q, J = 7.1 Hz, 2H), 1.42 (t, J = 7.1 Hz, 3H). ^{13}C NMR (100 MHz, $CDCl_3$) δ 164.7 (1C), 158.8 (1C), 135.3 (1C), 122.7 (1C), 60.6 (1C), 14.5 (1C).

7,8-dihydro-5H-pyrido[1,2-a]thiazolo[5,4-d] pyrimidin-10(6H)-one(5)

To the solution of compound 4 (1.7 g, 10 mmol) and piperidin-2-one (1.4 g, 12 mmol) in dry DCM (20 mL) was added $POCl_3$ (2.4 mL, 25 mmol) dropwise while cooled down to 0–5 °C. Then, the reaction mixture was stirred at reflux for 12 h. After completion of the reaction (monitored by TLC, eluent petroleum ether: ethyl acetate = 1:1, R_f = 0.34), the solvent and the excess of $POCl_3$ were evaporated under reduced pressure and the dark solid was suspended in DCM (100 mL) and was added NH_4OH (10%) up to pH = 9 and extracted with DCM (2 × 30 mL). The organic phase was washed with brine. The organic layer was separated and dried over anhydrous $MgSO_4$, filtered and concentrated under reduced pressure to give the crude product, which was purified by silica gel chromatography (petroleum ether/ethyl acetate = 1:1) to produce the pure corresponding compound 5 [36]. Yield 70%, light yellow solid, m p 234–235°C; ^{1}H NMR (400 MHz, $CDCl_3$) δ 8.74 (s, 1H), 4.14 (t, J = 6.1 Hz, 2H), 3.03 (t, J = 6.7 Hz, 2H), 2.24–1.81 (m, 4H). ^{13}C NMR (100 MHz, $CDCl_3$) δ 159.8 (1C), 157.2 (1C), 157.1 (1C), 150.2 (1C), 150.1 (1C), 42.7 (1C), 31.9 (1C), 21.8 (1C), 19.0 (1C).

2-bromo-7,8-dihydro-5H-pyrido[1,2-a]thiazolo[5,4-d] pyrimidin-10(6H)-one (6)

N-Bromosuccinimide (0.54 g, 3.03 mmol) was added to a solution of compound E (0.53 g, 2.53 mmol) in acetonitrile(20 mL), and the mixture was stirred for 30 min. After completion of the reaction (monitored by TLC, eluent petroleum ether: ethyl acetate = 5:1, R_f = 0.56), the reaction mixture was diluted with EtOAc (50 mL) and washed with 5% Na_2CO_3 solution (25 mL) followed by brine. The organic layer was dried over Na_2SO_4 and concentrated. The residue was purified by silica gel column chromatography to produce the pure corresponding compound F [37]. Yield 79%, light yellow solid, m p 226–227°C; ^{1}H NMR (400 MHz, $CDCl_3$) δ 4.06 (t, J = 6.1 Hz, 2H), 2.95 (t, J = 4.8 Hz, 2H), 2.38–1.82 (m, 4H). ^{13}C NMR (100 MHz, $CDCl_3$) δ 161.1 (1C), 157.8 (1C), 155.8 (1C), 149.1 (1C), 134.2 (1C), 42.9 (1C), 31.9 (1C), 21.7 (1C), 18.9 (1C).

General procedure of preparation of 7a-7an

A solution of 2-bromo-7,8-dihydro-5*H*-pyrido[1,2-*a*]thiazolo[5,4-*d*]pyrimidin-10(6*H*)-one(6) (285 mg, 1 mmol), substituted phenylboronic acid (1.2 mmol), potassium carbonate (414 mg, 3 mmol) and tetrakis(triphenylphosphine) palladium (58 mg, 0.05 mmol) in oxygen-free toluene/water (3:1) (8 mL) was heated at 110℃ for 24 h. After completion of the reaction (monitored by TLC, eluent petroleum ether: ethyl acetate = 1:2, $R_f$values between 0.36 and 0.59), the reaction mixture was cooled to rt and quenched with ethyl acetate. The aqueous layer was extracted with ethyl acetate. The combined organic layers were washed with brine, dried over magnesium sulfate, filtered and concentrated under reduced pressure. The residue was purified on silica gel (petroleum ether/ethyl acetate = 1:2) and afforded the desired products 7a-7an [38].

2-phenyl-7,8-dihydro-5H-pyrido[1,2-a]thiazolo[5,4-d] pyrimidin-10(6H)-one(7a) Yield 83%, light yellow solid, m p 198–199 °C, HPLC purity: > 98%. ^{1}H NMR (400 MHz, $CDCl_3$) δ 8.21–7.90 (m, 2H), 7.56–7.35 (m, 3H), 4.13 (t, J = 6.1 Hz, 2H), 3.00 (dd, J = 9.1, 4.2 Hz, 2H), 2.20–1.68 (m, 4H). ^{13}C NMR(100 MHz, $CDCl_3$) δ 164.3 (1C), 160.2 (1C), 157.0 (1C), 156.7 (1C), 136.7 (1C), 133.0 (1C), 131.0 (1C), 128.9 (2C), 127.3 (2C), 42.8 (1C), 31.9 (1C), 21.8 (1C), 19.1 (1C). HRMS (ESI) calcd for $C_{15}H_{15}N_3OS$ $[M+H]^+$ 284.0844, found 284.0852.

2-(o-tolyl)-7,8-dihydro-5H-pyrido[1,2-a]thiazolo[5,4-d] pyrimidin-10(6H)-one(7b) Yield 69%, light yellow solid, m p 180–181 °C, HPLC purity: > 98%. ^{1}H NMR (400 MHz, $CDCl_3$) δ 7.74 (d, J = 7.7 Hz, 1H), 7.38–7.26 (m, 3H), 4.16 (t, J = 6.2 Hz, 2H), 3.03 (t, J = 6.7 Hz, 2H), 2.65 (s, 3H), 2.10–1.91 (m, 4H). ^{13}C NMR (100 MHz, $CDCl_3$) δ 164.2 (1C), 160.6 (1C), 157.0 (1C), 156.6 (1C), 137.2 (1C), 136.2 (1C), 132.4 (1C), 131.5 (1C), 130.4 (1C), 130.1 (1C), 126.0 (1C), 42.7 (1C), 31.9 (1C), 21.9 (1C), 21.5 (1C), 19.1 (1C). HRMS (ESI) calcd for $C_{16}H_{17}N_3OS$ $[M+H]^+$ 298.1003, found 298.1009.

2-(m-tolyl)-7,8-dihydro-5H-pyrido[1,2-a]thiazolo[5,4-d] pyrimidin-10(6H)-one(7c) Yield 74%, light yellow solid, m p 206–207 °C, HPLC purity: > 98%. ^{1}H NMR (400 MHz, $CDCl_3$) δ 7.94 (s, 1H), 7.81 (d, J = 7.7 Hz, 1H), 7.34 (t, J = 7.6 Hz, 1H), 7.27 (d, J = 8.6 Hz, 1H), 4.15 (t, J = 6.2 Hz, 2H), 3.02 (t, J = 6.7 Hz, 2H), 2.42 (s, 3H), 2.09–1.87 (m, 4H). ^{13}C NMR (100 MHz, $CDCl_3$) δ 164.6 (1C), 160.2 (1C), 157.0 (1C), 156.7 (1C), 138.8 (1C), 136.7 (1C), 133.0 (1C), 131.9 (1C), 128.8 (1C), 127.8 (1C), 124.5 (1C), 42.8 (1C), 31.9 (1C), 21.9 (1C), 21.3 (1C), 19.1 (1C). HRMS (ESI) calcd for $C_{16}H_{17}N_3OS$ $[M+H]^+$ 298.1004, found 298.1009.

2-(p-tolyl)-7,8-dihydro-5H-pyrido[1,2-a]thiazolo[5,4-d]pyrimidin-10(6H)-one(7d) Yield 77%, light yellow solid, m p 256–257 °C, HPLC purity: > 98%. ^{1}H NMR (400 MHz, $CDCl_3$) δ 7.95 (d, J = 8.2 Hz, 2H), 7.25 (d, J = 7.9 Hz, 2H), 4.14 (t, J = 6.2 Hz, 2H), 3.01 (t, J = 6.7 Hz, 2H), 2.40 (s, 3H), 2.18–1.82 (m, 4H). ^{13}C NMR (100 MHz, $CDCl_3$) δ 164.6 (1C), 160.1 (1C), 157.0 (1C), 156.6 (1C), 141.5 (1C), 136.7 (1C), 130.5 (1C), 129.6 (2C), 127.2 (2C), 42.8 (1C), 31.9 (1C), 21.9 (1C), 21.5 (1C), 19.1 (1C). HRMS (ESI) calcd for $C_{16}H_{17}N_3OS$ $[M+H]^+$ 298.1004, found 298.1009.

2-(4-(tert-butyl)phenyl)-7,8-dihydro-5H-pyrido[1,2-a]thiazolo[5,4-d]pyrimidin-10(6H)-one(7e) Yield 78%, light yellow solid, m p 249–250 °C, HPLC purity: > 98%. ^{1}H NMR (400 MHz, $CDCl_3$) δ 8.00 (d, J = 8.2 Hz, 2H), 7.47 (d, J = 8.3 Hz, 2H), 4.15 (t, J = 6.0 Hz, 2H), 3.02 (t, J = 6.5 Hz, 2H), 2.18–1.70 (m, 4H), 1.35 (s, 9H). ^{13}C NMR (100 MHz, $CDCl_3$) δ 164.4 (1C), 160.1 (1C), 157.0 (1C), 156.5 (1C), 154.6 (1C), 136.7 (1C), 130.4 (1C), 127.0 (2C), 125.9 (2C), 42.7 (1C), 34.9 (1C), 31.9 (1C), 31.1 (3C), 21.9 (1C), 19.1 (1C). HRMS (ESI) calcd for $C_{19}H_{23}N_3OS$ $[M+H]^+$ 340.1472, found 340.1478.

2-(2-chlorophenyl)-7,8-dihydro-5H-pyrido[1,2-a]thiazolo[5,4-d]pyrimidin-10(6H)-one(7f) Yield 65%, light yellow solid, m p 179–180 °C, HPLC purity: > 98%. ^{1}H NMR (400 MHz, $CDCl_3$) δ 8.42–8.37 (m, 1H), 7.49 (d, J = 2.6 Hz, 1H), 7.42–7.35 (m, 2H), 4.16 (t, J = 5.3 Hz, 2H), 3.04 (t, J = 6.4 Hz, 2H), 2.18–1.86 (m, 4H). ^{13}C NMR (100 MHz, $CDCl_3$) δ 161.0 (1C), 159.9 (1C), 157.1 (1C), 157.0 (1C), 135.1 (1C), 132.1 (1C), 131.6 (1C), 131.5 (1C), 131.2 (1C), 130.6 (1C), 127.1 (1C), 42.7 (1C), 31.9 (1C), 21.9 (1C), 19.1 (1C). HRMS (ESI) calcd for $C_{15}H_{14}ClN_3OS$ $[M+H]^+$ 318.0458, found 318.0462.

2-(3-chlorophenyl)-7,8-dihydro-5H-pyrido[1,2-a]thiazolo[5,4-d]pyrimidin-10(6H)-one(7 g) Yield 74%, light yellow solid, m p 217–218 °C, HPLC purity: > 98%. ^{1}H NMR (400 MHz, $CDCl_3$) δ 8.11 (t, J = 1.7 Hz, 1H), 7.91 (dt, J = 7.4, 1.5 Hz, 1H), 7.45–7.37 (m, 2H), 4.15 (t, J = 6.2 Hz, 2H), 3.03 (t, J = 6.7 Hz, 2H), 2.28–1.76 (m, 4H). ^{13}C NMR (100 MHz, $CDCl_3$) δ 162.5 (1C), 160.5 (1C), 157.1 (1C), 156.9 (1C), 135.1 (1C), 134.6 (1C), 130.9 (1C), 130.1 (1C), 127.1 (1C), 125.3 (1C), 109.6 (1C), 42.8 (1C), 31.9 (1C), 21.8 (1C), 19.0 (1C). HRMS (ESI) calcd for $C_{15}H_{14}ClN_3OS$ $[M+H]^+$ 318.0457, found 318.0462.

2-(4-chlorophenyl)-7,8-dihydro-5H-pyrido[1,2-a]thiazolo[5,4-d]pyrimidin-10(6H)-one(7 h) Yield 71%, light yellow solid, m p 230–231 °C, HPLC purity: > 98%. ^{1}H NMR (400 MHz, $CDCl_3$) δ 8.00 (d, J = 8.6 Hz, 2H), 7.44 (d, J = 8.6 Hz, 2H), 4.15 (t, J = 6.2 Hz, 2H), 3.03 (t, J = 6.7 Hz, 2H), 2.30–1.78 (m, 4H). ^{13}C NMR (100 MHz, $CDCl_3$) δ 162.9 (1C), 160.4 (1C), 157.0 (1C), 156.9 (1C), 137.1 (1C), 136.8 (1C), 131.6 (1C), 129.2 (2C), 128.5 (2C), 42.8 (1C), 31.9 (1C), 21.8 (1C), 19.1 (1C). HRMS (ESI) calcd for $C_{15}H_{14}ClN_3OS$ $[M+H]^+$ 318.0458, found 318.0462.

2-(2-bromophenyl)-7,8-dihydro-5H-pyrido[1,2-a]thiazolo[5,4-d]pyrimidin-10(6H)-one(7i) Yield 60%, light yellow solid, m p 167–168 °C, HPLC purity: > 98%. ^{1}H NMR (400 MHz, $CDCl_3$) δ 8.18 (dd, J = 7.9, 1.7 Hz, 1H), 7.68 (dd, J = 8.0, 1.0 Hz, 1H), 7.41 (td, J = 7.7, 1.2 Hz, 1H), 7.29 (td, J = 7.7, 1.7 Hz, 1H), 4.15 (t, J = 6.2 Hz, 2H), 3.03 (t, J = 6.7 Hz, 2H), 2.28–1.82 (m, 4H). ^{13}C NMR (100 MHz, $CDCl_3$) δ 161.5 (1C), 161.1 (1C), 157.2 (1C), 157.1 (1C), 135.3 (1C), 133.9 (1C), 133.7 (1C), 132.4 (1C), 131.4 (1C), 127.6 (1C), 121.7 (1C), 42.8 (1C), 31.9 (1C), 21.9 (1C), 19.1 (1C). HRMS (ESI) calcd for $C_{15}H_{14}BrN_3OS$ $[M+H]^+$ 361.9949, found 361.9957.

2-(3-bromophenyl)-7,8-dihydro-5H-pyrido[1,2-a]thiazolo[5,4-d]pyrimidin-10(6H)-one(7j) Yield 74%, light yellow solid, m p 234–235 °C, HPLC purity: > 98%. ^{1}H NMR (400 MHz, $CDCl_3$) δ 8.26 (t, J = 1.8 Hz, 1H), 8.03–7.84 (m, 1H), 7.58 (ddd, J = 7.9, 1.8, 0.9 Hz, 1H), 7.32 (t, J = 7.9 Hz, 1H), 4.14 (t, J = 6.2 Hz, 2H), 3.02 (t, J = 6.7 Hz, 2H), 2.41–1.78 (m, 4H). ^{13}C NMR (100 MHz, $CDCl_3$) δ 162.4 (1C), 160.5 (1C), 157.1 (1C), 156.9 (1C), 134.9 (1C), 133.8 (1C), 130.4 (1C), 129.9 (1C), 125.8 (1C), 123.1 (1C), 109.3 (1C), 42.8 (1C), 31.9 (1C), 21.8 (1C), 19.0 (1C). HRMS (ESI) calcd for $C_{15}H_{14}BrN_3OS$ $[M+H]^+$ 361.9948, found 361.9957.

2-(4-bromophenyl)-7,8-dihydro-5H-pyrido[1,2-a]thiazolo[5,4-d]pyrimidin-10(6H)-one(7 k) Yield 72%, light yellow solid, m p 226–227 °C, HPLC purity: > 98%. ^{1}H NMR (400 MHz, $CDCl_3$) δ 7.91 (d, J = 8.6 Hz, 2H), 7.58 (d, J = 8.7 Hz, 2H), 4.13 (t, J = 6.2 Hz, 2H), 3.01 (t, J = 6.7 Hz, 2H), 2.17–1.85 (m, 4H). ^{13}C NMR (100 MHz, $CDCl_3$) δ 162.9 (1C), 160.4 (1C), 157.0 (1C), 156.9 (1C), 136.8 (1C), 132.2 (1C), 132.0 (2C), 128.6 (2C), 125.5 (1C), 42.9 (1C), 31.9 (1C), 21.8 (1C), 19.1 (1C). HRMS (ESI) calcd for $C_{15}H_{14}BrN_3OS$ $[M+H]^+$ 361.9956, found 361.9957.

2-(2-fluorophenyl)-7,8-dihydro-5H-pyrido[1,2-a]thiazolo[5,4-d]pyrimidin-10(6H)-one(7 l) Yield 58%, light yellow solid, m p 248–249 °C, HPLC purity: > 98%. ^{1}H NMR (400 MHz, $CDCl_3$) δ 8.52 (t, J = 7.6 Hz, 1H), 7.45 (dd, J = 13.1, 6.3 Hz, 1H), 7.31 (dd, J = 11.6, 7.5 Hz, 1H), 7.21 (dd, J = 11.2, 8.6 Hz, 1H), 4.17 (t, J = 6.1 Hz, 2H), 3.05 (t, J = 6.6 Hz, 2H), 2.30–1.80 (m, 4H). ^{13}C NMR (100 MHz, $CDCl_3$) δ 160.9 (1C), 160.2 (dd, J = 250.6, 6.3 Hz) (1C), 157.2 (1C), 157.0 (1C), 156.9 (1C), 135.3 (1C), 134.2 (d, J = 10.7 Hz) (1C), 132.2 (d, J = 7.2 Hz) (1C), 128.5 (d, J = 12.1 Hz) (1C), 124.7 (1C), 120.9 (d,

$J = 10.2$ Hz) (1C), 116.1 (d, $J = 21.7$ Hz) (1C), 42.8 (1C), 31.9 (1C), 21.9 (1C), 19.1 (1C). HRMS (ESI) calcd for $C_{15}H_{14}FN_3OS$ $[M+H]^+$ 302.0751, found 302.0752.

2-(4-fluorophenyl)-7,8-dihydro-5H-pyrido[1,2-a]thiazolo[5,4-d]pyrimidin-10(6H)-one(7 m) Yield 69%, light yellow solid, m p 255–256 °C, HPLC purity: > 98%. ^{1}H NMR (400 MHz, $CDCl_3$) δ 8.06 (dd, $J = 8.6$, 5.3 Hz, 2H), 7.15 (t, $J = 8.6$ Hz, 2H), 4.15 (t, $J = 6.2$ Hz, 2H), 3.03 (t, $J = 6.6$ Hz, 2H), 2.15–1.79 (m, 4H). ^{13}C NMR (100 MHz, $CDCl_3$) δ 164.4 (d, $J = 252.4$ Hz) (1C), 163.1 (1C), 160.3 (1C), 156.9 (1C), 156.8 (1C), 136.7 (1C), 129.4 (d, $J = 3.5$ Hz) (1C), 129.3 (d, $J = 8.6$ Hz) (2C), 116.1 (d, $J = 22.2$ Hz) (2C), 42.8 (1C), 31.9 (1C), 21.8 (1C), 19.1 (1C). HRMS (ESI) calcd for $C_{15}H_{14}FN_3OS$ $[M+H]^+$ 302.0750, found 302.0752.

2-(2-(trifluoromethyl)phenyl)-7,8-dihydro-5H-pyrido[1,2-a]thiazolo[5,4-d]pyrimidin-10(6H)-one(7n) Yield 59%, light yellow solid, m p 108–109 °C, HPLC purity: > 98%. ^{1}H NMR (400 MHz, $CDCl_3$) δ 7.80 (d, $J = 7.2$ Hz, 1H), 7.70 (d, $J = 7.4$ Hz, 1H), 7.68–7.58 (m, 2H), 4.16 (t, $J = 6.1$ Hz, 2H), 3.04 (t, $J = 6.6$ Hz, 2H), 2.38–1.83 (m, 4H). ^{13}C NMR (100 MHz, $CDCl_3$) δ 161.6 (1C), 160.7 (1C), 157.2 (1C), 156.9 (1C), 135.9 (1C), 132.5 (1C), 132.0 (1C), 131.7 (1C), 130.3 (1C), 126.6 (q, $J = 5.2$ Hz) (1C), 124.8 (1C), 122.1 (1C), 42.8 (1C), 31.9 (1C), 21.8 (1C), 19.0 (1C). HRMS (ESI) calcd for $C_{16}H_{14}F_3N_3OS$ $[M+H]^+$ 352.0719, found 352.0726.

2-(4-(trifluoromethyl)phenyl)-7,8-dihydro-5H-pyrido[1,2-a]thiazolo[5,4-d]pyrimidin-10(6H)-one(7o) Yield 57%, light yellow solid, m p 201–202 °C, HPLC purity: > 98%. ^{1}H NMR (400 MHz, $CDCl_3$) δ 8.18 (d, $J = 8.2$ Hz, 2H), 7.72 (d, $J = 8.2$ Hz, 2H), 4.16 (t, $J = 6.1$ Hz, 2H), 3.04 (t, $J = 6.6$ Hz, 2H), 2.21–1.84 (m, 4H). ^{13}C NMR (100 MHz, $CDCl_3$) δ 162.3 (1C), 160.7 (1C), 157.4 (1C), 156.9 (1C), 136.5 (d, $J = 75.6$ Hz) (1C), 134.2 (d, $J = 13.7$ Hz) (1C), 132.3 (1C), 128.4 (d, $J = 9.2$ Hz) (1C), 127.5 (2C), 125.9 (q, $J = 3.7$ Hz) (1C), 123.7 (d, $J = 272.4$ Hz) (1C), 42.9 (1C), 31.9 (1C), 21.8 (1C), 19.0 (1C). HRMS (ESI) calcd for $C_{16}H_{14}F_3N_3OS$ $[M+H]^+$ 352.0701, found 352.0726.

2-(3-methoxyphenyl)-7,8-dihydro-5H-pyrido[1,2-a]thiazolo[5,4-d]pyrimidin-10(6H)-one(7p) Yield 66%, light yellow solid, m p 202–203 °C, HPLC purity: > 98%. ^{1}H NMR (400 MHz, $CDCl_3$) δ 7.67 (s, 1H), 7.56 (d, $J = 7.7$ Hz, 1H), 7.35 (t, $J = 8.0$ Hz, 1H), 7.01 (dd, $J = 8.2$, 2.1 Hz, 1H), 4.14 (t, $J = 6.1$ Hz, 2H), 3.89 (s, 3H), 3.02 (t, $J = 6.6$ Hz, 2H), 2.39–1.80 (m, 4H). ^{13}C NMR (100 MHz, $CDCl_3$) δ 164.2 (1C), 160.3 (1C), 159.9 (1C), 157.0 (1C), 156.7 (1C), 136.6 (1C), 134.3 (1C), 129.9 (1C), 119.9 (1C), 117.7 (1C), 111.3 (1C), 55.6 (1C), 42.8 (1C), 31.9 (1C), 21.8 (1C), 19.1 (1C). HRMS (ESI) calcd for $C_{16}H_{17}N_3O_2S$ $[M+H]^+$ 314.0950, found 314.0958.

2-(4-methoxyphenyl)-7,8-dihydro-5H-pyrido[1,2-a]thiazolo[5,4-d]pyrimidin-10(6H)-one(7q) Yield 76%, light yellow solid, m p 196–197 °C, HPLC purity: > 98%. ^{1}H NMR (400 MHz, $CDCl_3$) δ 8.01 (d, $J = 8.8$ Hz, 2H), 6.97 (d, $J = 8.8$ Hz, 2H), 4.46 4.04 (m, 2H), 3.87 (s, 3H), 3.02 (t, $J = 6.6$ Hz, 2H), 2.06–1.93 (m, 4H). ^{13}C NMR (100 MHz, $CDCl_3$) δ 164.3 (1C), 161.9 (1C), 159.8 (1C), 156.9 (1C), 156.3 (1C), 136.6 (1C), 128.8 (2C), 125.9 (1C), 114.3 (2C), 55.5 (1C), 42.8 (1C), 31.9 (1C), 21.8 (1C), 19.1 (1C). HRMS (ESI) calcd for $C_{16}H_{17}N_3O_2S$ $[M+H]^+$ 314.0950, found 314.0958.

2-(10-oxo-6,7,8,10-tetrahydro-5H-pyrido[1,2-a]thiazolo[5,4-d]pyrimidin-2-yl)benzonitrile(7r) Yield 55%, light yellow solid, m p 179–180 °C, HPLC purity: > 98%. ^{1}H NMR (400 MHz, $CDCl_3$) δ 8.28 (d, $J = 8.0$ Hz, 1H), 7.82 (d, $J = 7.9$ Hz, 1H), 7.72 (t, $J = 7.8$ Hz, 1H), 7.57 (t, $J = 7.6$ Hz, 1H), 4.17 (t, $J = 6.1$ Hz, 2H), 3.05 (t, $J = 6.6$ Hz, 2H), 1.96–2.06 (m, 4H). ^{13}C NMR (100 MHz, $CDCl_3$) δ 162.5 (1C), 160.9 (1C), 157.7 (1C), 156.9 (1C), 135.8 (1C), 134.6 (1C), 134.5 (1C), 132.9 (1C), 130.4 (1C), 130.2 (1C), 117.9 (1C), 110.5 (1C), 42.9 (1C), 31.9 (1C), 21.8 (1C), 19.0 (1C). HRMS (ESI) calcd for $C_{16}H_{14}N_4OS$ $[M+H]^+$ 309.0800, found 309.0805.

3-(10-oxo-6,7,8,10-tetrahydro-5H-pyrido[1,2-a]thiazolo[5,4-d]pyrimidin-2-yl)benzonitrile(7 s) Yield 67%, light yellow solid, m p 231–232 °C, HPLC purity: > 98%. ^{1}H NMR (400 MHz, $CDCl_3$) δ 8.35 (s, 1H), 8.27 (d, $J = 7.9$ Hz, 1H), 7.73 (d, $J = 7.5$ Hz, 1H), 7.59 (t, $J = 7.8$ Hz, 1H), 4.15 (t, $J = 5.6$ Hz, 2H), 3.03 (t, $J = 6.5$ Hz, 2H), 2.05–1.96 (m 4H). ^{13}C NMR (100 MHz, $CDCl_3$) δ 161.2 (1C), 160.7 (1C), 157.6 (1C), 156.9 (1C), 136.8 (1C), 134.2 (1C), 133.8 (1C), 131.0 (1C), 130.5 (1C), 129.9 (1C), 117.8 (1C), 113.4 (1C), 42.9 (1C), 31.9 (1C), 21.8 (1C), 18.9 (1C). HRMS (ESI) calcd for $C_{16}H_{14}N_4OS$ $[M+H]^+$ 309.0800, found 309.0805.

4-(10-oxo-6,7,8,10-tetrahydro-5H-pyrido[1,2-a]thiazolo[5,4-d]pyrimidin-2-yl)benzonitrile(7t) Yield 68%, light yellow solid, m p 169–170 °C, HPLC purity: > 98%. ^{1}H NMR (400 MHz, $CDCl_3$) δ 8.17 (d, $J = 7.6$ Hz, 2H), 7.76 (d, $J = 7.6$ Hz, 2H), 4.16 (t, $J = 5.4$ Hz, 2H), 3.05 (t, $J = 6.4$ Hz, 2H), 2.25–1.88 (m, 4H). ^{13}C NMR (100 MHz, $CDCl_3$) δ 161.5 (1C), 160.9 (1C), 157.6 (1C), 156.9 (1C), 136.9 (1C), 136.8 (1C), 132.7 (2C), 127.6 (2C), 118.2 (1C), 114.1 (1C), 42.9 (1C), 31.9 (1C), 21.8 (1C), 18.9 (1C). HRMS (ESI) calcd for $C_{16}H_{14}N_4OS$ $[M+H]^+$ 309.0798, found 309.0805.

4-(10-oxo-6,7,8,10-tetrahydro-5H-pyrido[1,2-a]thiazolo[5,4-d]pyrimidin-2-yl)benzaldehyde(7u) Yield

73%, light yellow solid, m p 171–172 °C, HPLC purity: > 98%. ^{1}H NMR (400 MHz, $CDCl_3$) δ 10.07 (s, 1H), 8.24 (d, J = 8.2 Hz, 2H), 7.98 (d, J = 8.2 Hz, 2H), 4.16 (t, J = 6.1 Hz, 2H), 3.05 (t, J = 6.6 Hz, 2H), 2.32–1.81 (m, 4H). ^{13}C NMR (100 MHz, $CDCl_3$) δ 191.4 (1C), 162.3 (1C), 160.8 (1C), 157.5 (1C), 156.9 (1C), 138.0 (1C), 137.6 (1C), 137.0 (1C), 130.2 (2C), 127.7 (2C), 42.9 (1C), 31.9 (1C), 21.8 (1C), 19.0 (1C). HRMS (ESI) calcd for $C_{16}H_{15}N_3O_2S$ $[M+H]^+$ 312.0793, found 312.0801.

2-(3-acetylphenyl)-7,8-dihydro-5H-pyrido[1,2-a] thiazolo[5,4-d]pyrimidin-10(6H)-one(7v) Yield 80%, light yellow solid, m p 195–196 °C, HPLC purity: > 98%. ^{1}H NMR (400 MHz, $CDCl_3$) δ 8.52 (s, 1H), 8.20 (dd, J = 7.8, 0.8 Hz, 1H), 8.00 (d, J = 7.8 Hz, 1H), 7.53 (t, J = 7.8 Hz, 1H), 4.10 (t, J = 6.2 Hz, 2H), 2.99 (t, J = 6.6 Hz, 2H), 2.65 (s, 3H), 2.08–1.88 (m, 4H). ^{13}C NMR (100 MHz, $CDCl_3$) δ 197.4 (1C), 163.0 (1C), 160.5 (1C), 157.2 (1C), 156.9 (1C), 137.7 (1C), 136.7 (1C), 133.6 (1C), 131.5 (1C), 130.4 (1C), 129.3 (1C), 126.9 (1C), 42.9 (1C), 31.9 (1C), 26.9 (1C), 21.8 (1C), 19.0 (1C). HRMS (ESI) calcd for $C_{17}H_{17}N_3O_2S$ $[M+H]^+$ 326.0950, found 326.0958.

2-(3-nitrophenyl)-7,8-dihydro-5H-pyrido[1,2-a] thiazolo[5,4-d]pyrimidin-10(6H)-one(7w) Yield 63%, light yellow solid, m p 261–262 °C, HPLC purity: > 98%. ^{1}H NMR (400 MHz, $CDCl_3$) δ 8.85 (s, 1H), 8.43 (d, J = 7.8 Hz, 1H), 8.32 (dd, J = 8.2, 1.1 Hz, 1H), 7.67 (t, J = 8.0 Hz, 1H), 4.16 (t, J = 6.1 Hz, 2H), 3.05 (t, J = 6.6 Hz, 2H), 2.49–1.75 (m, 4H). ^{13}C NMR (100 MHz, $CDCl_3$) δ 161.1 (1C), 160.8 (1C), 157.6 (1C), 156.9 (1C), 148.6 (1C), 136.8 (1C), 134.6 (1C), 132.7 (1C), 130.1 (1C), 125.2 (1C), 121.9 (1C), 42.9 (1C), 31.9 (1C), 21.8 (1C), 19.0 (1C). HRMS (ESI) calcd for $C_{15}H_{14}N_4O_3S$ $[M+H]^+$ 329.0697, found 329.0703.

2-(3,5-dimethylphenyl)-7,8-dihydro-5H-pyrido[1,2-a] thiazolo[5,4-d]pyrimidin-10(6H)-one(7x) Yield 70%, light yellow solid, m p 258–259 °C, HPLC purity: > 98%. ^{1}H NMR (400 MHz, $CDCl_3$) δ 7.70 (s, 2H), 7.10 (s, 1H), 4.15 (t, J = 6.1 Hz, 2H), 3.03 (t, J = 6.6 Hz, 2H), 2.38 (s, 6H), 2.24–1.80 (m, 4H). ^{13}C NMR (100 MHz, $CDCl_3$) δ 164.8 (1C), 160.0 (1C), 157.0 (1C), 156.5 (1C), 138.6 (2C), 136.6 (1C), 132.8 (2C), 132.8 (1C), 125.0 (2C), 42.8 (1C), 31.9 (1C), 21.9 (1C), 21.1 (1C), 19.1 (1C). HRMS (ESI) calcd for $C_{17}H_{19}N_3OS$ $[M+H]^+$ 312.1167, found 312.1165.

2-(3,5-dichlorophenyl)-7,8-dihydro-5H-pyrido[1,2-a] thiazolo[5,4-d]pyrimidin-10(6H)-one(7y) Yield 72%, light yellow solid, m p 271–272 °C, HPLC purity: > 98%. ^{1}H NMR (400 MHz, $CDCl_3$) δ 7.94 (d, J = 1.5 Hz, 2H), 7.42 (t, J = 1.6 Hz, 1H), 4.14 (t, J = 6.1 Hz, 2H), 3.02 (t, J = 6.6 Hz, 2H), 2.32–1.74 (m, 4H). ^{13}C NMR (100 MHz, $CDCl_3$) δ 160.8 (1C), 160.7 (1C), 157.5 (1C), 156.9 (1C), 136.7 (1C), 135.7 (1C), 135.6 (1C), 130.6 (2C), 125.4 (2C), 42.9 (1C), 31.9 (1C), 21.8 (1C), 19.0 (1C). HRMS (ESI) calcd for $C_{15}H_{13}Cl_2N_3OS$ $[M+H]^+$ 352.0065, found 352.0073.

2-(3,4-dichlorophenyl)-7,8-dihydro-5H-pyrido[1,2-a] thiazolo[5,4-d]pyrimidin-10(6H)-one(7z) Yield 77%, light yellow solid, m p 218–220 °C, HPLC purity: > 98%. ^{1}H NMR (400 MHz, $CDCl_3$) δ 8.19 (s, 1H), 7.85 (d, J = 8.4 Hz, 1H), 7.52 (d, J = 8.4 Hz, 1H), 4.14 (t, J = 6.1 Hz, 2H), 3.03 (t, J = 6.6 Hz, 2H), 2.11–1.88 (m, 4H). ^{13}C NMR(100 MHz, $CDCl_3$) δ 161.4 (1C), 160.6 (1C), 157.4 (1C), 156.9 (1C), 136.8 (1C), 135.1 (1C), 133.5 (1C), 132.9 (1C), 130.9 (1C), 128.7 (1C), 126.2 (1C), 42.9 (1C), 31.9 (1C), 21.8 (1C), 19.0 (1C). HRMS (ESI) calcd for $C_{15}H_{13}Cl_2N_3OS$ $[M+H]^+$ 352.0074, found 352.0073.

2-(3,5-dibromophenyl)-7,8-dihydro-5H-pyrido[1,2-a] thiazolo[5,4-d]pyrimidin-10(6H)-one(7aa) Yield 79%, light yellow solid, m p 261–262 °C, HPLC purity: > 98%. ^{1}H NMR (400 MHz, $CDCl_3$) δ 8.12 (s, 2H), 7.72 (s, 1H), 4.13 (t, J = 6.1 Hz, 2H), 3.02 (t, J = 6.6 Hz, 2H), 2.33–1.76 (m, 4H). ^{13}C NMR (100 MHz, $CDCl_3$) δ 160.7 (1C), 160.5 (1C), 157.5 (1C), 156.9 (1C), 136.7 (1C), 136.1 (1C), 136.0 (2C), 128.6 (2C), 123.5 (1C), 42.9 (1C), 31.9 (1C), 21.8 (1C), 19.0 (1C). HRMS (ESI) calcd for $C_{15}H_{13}Br_2N_3OS$ $[M+H]^+$ 439.9060, found 439.9062.

2-(3,5-difluorophenyl)-7,8-dihydro-5H-pyrido[1,2-a] thiazolo[5,4-d]pyrimidin-10(6H)-one(7ab) Yield 71%, light yellow solid, m p 248–249 °C, HPLC purity: > 98%. ^{1}H NMR (400 MHz, CDCl3) δ 7.57 (d, J = 6.4 Hz, 2H), 6.89 (td, J = 8.6, 2.2 Hz, 1H), 4.12 (t, J = 6.1 Hz, 2H), 3.01 (t, J = 6.6 Hz, 2H), 2.30–1.76 (m, 4H). ^{13}C NMR (100 MHz, $CDCl_3$) δ 163.2 (dd, J = 250.0, 12.6 Hz) (1C), 161.2 (1C), 160.7 (1C), 157.5 (1C), 156.9 (1C), 136.7 (1C), 135.9 (t, J = 10.1 Hz) (1C), 110.6 (dd, J = 27.7, 11.6 Hz) (2C), 106.1 (t, J = 25.3 Hz) (2C), 42.9 (1C), 31.9 (1C), 21.8 (1C), 19.0 (1C). HRMS (ESI) calcd for $C_{15}H_{13}F_2N_3OS$ $[M+H]^+$ 320.0654, found 320.0664.

2-(3,5-dimethoxyphenyl)-7,8-dihydro-5H-pyrido[1,2-a] thiazolo[5,4-d]pyrimidin-10(6H)-one(7ac) Yield 58%, light yellow solid, m p 223–224 °C, HPLC purity: > 98%. ^{1}H NMR (400 MHz, $CDCl_3$) δ 7.20 (d, J = 1.8 Hz, 2H), 6.56 (s, 1H), 4.15 (t, J = 6.1 Hz, 2H), 3.87 (s, 6H), 3.03 (t, J = 6.6 Hz, 2H), 2.30–1.83 (m, 4H). ^{13}C NMR (100 MHz, $CDCl_3$) δ 164.2 (1C), 161.0 (2C), 160.3 (1C), 157.0 (1C), 156.8 (1C), 136.6 (1C), 134.8 (1C), 105.1 (2C), 103.6 (2C), 55.7 (1C), 42.8 (1C), 31.9 (1C), 21.8 (1C), 19.1 (1C). HRMS (ESI) calcd for $C_{17}H_{19}N_3O_3S$ $[M+H]^+$ 344.1041, found 344.1063.

2-(3,4-dimethoxyphenyl)-7,8-dihydro-5H-pyrido[1,2-a]thiazolo[5,4-d]pyrimidin-10(6H)-one(7ad) Yield 63%, light yellow solid, m p 216–217 °C, HPLC purity: > 98%. ^{1}H NMR (400 MHz, $CDCl_3$) δ 7.70 (d, J = 1.3 Hz, 1H), 7.49 (dd, J = 8.4, 1.4 Hz, 1H), 6.90 (d, J = 8.4 Hz, 1H), 4.14 (t, J = 6.1 Hz, 2H), 3.99 (s, 3H), 3.93 (s, 3H), 3.01 (t, J = 6.6 Hz, 2H), 2.12–1.88 (m, 4H). ^{13}C NMR (100 MHz, $CDCl_3$) δ 164.3 (1C), 159.9 (1C), 157.0 (1C), 156.4 (1C), 151.5 (1C), 149.3 (1C), 136.6 (1C), 126.2 (1C), 120.9 (1C), 110.7 (1C), 109.3 (1C), 56.3 (1C), 56.0 (1C), 42.8 (1C), 31.8 (1C), 21.8 (1C), 19.1 (1C). HRMS (ESI) calcd for $C_{17}H_{19}N_3O_3S$ $[M+H]^+$ 344.1056, found 344.1063.

2-(3-chloro-4-fluorophenyl)-7,8-dihydro-5H-pyrido[1,2-a]thiazolo[5,4-d]pyrimidin-10(6H)-one(7ae) Yield 57%, light yellow solid, m p 257–258 °C, HPLC purity: > 98%. ^{1}H NMR (400 MHz, $CDCl_3$) δ 8.17 (dd, J = 6.9, 2.0 Hz, 1H), 8.05–7.63 (m, 1H), 7.22 (t, J = 8.6 Hz, 1H), 4.15 (t, J = 6.1 Hz, 2H), 3.03 (t, J = 6.6 Hz, 2H), 2.53–1.73 (m, 4H). ^{13}C NMR (100 MHz, $CDCl_3$) δ 161.5 (1C), 160.5 (1C), 159.6 (d, J = 254.5 Hz) (1C), 157.2 (1C), 156.9 (1C), 136.7 (1C), 130.3 (d, J = 3.8 Hz) (1C), 129.4 (1C), 127.1 (d, J = 7.7 Hz) (1C), 122.1 (d, J = 18.3 Hz) (1C), 117.1 (d, J = 21.9 Hz) (1C), 42.9 (1C), 31.9 (1C), 21.8 (1C), 19.0 (1C). HRMS (ESI) calcd for $C_{15}H_{12}ClFN_3OS$ $[M+H]^+$ 336.0361, found 336.0368.

2-(furan-3-yl)-7,8-dihydro-5H-pyrido[1,2-a]thiazolo[5,4-d]pyrimidin-10(6H)-one(7af) Yield 69%, light yellow solid, m p 187–188 °C, HPLC purity: > 98%. ^{1}H NMR (400 MHz, $CDCl_3$) δ 8.10 (s, 1H), 7.50 (d, J = 1.5 Hz, 1H), 6.97 (d, J = 1.0 Hz, 1H), 4.14 (t, J = 6.1 Hz, 2H), 3.02 (t, J = 6.7 Hz, 2H), 2.49–1.70 (m, 4H). ^{13}C NMR (100 MHz, $CDCl_3$) δ 159.6 (1C), 156.8 (1C), 156.6 (1C), 156.6 (1C), 144.1 (1C), 142.5 (1C), 121.5 (1C), 109.9 (1C), 109.1 (1C), 42.8 (1C), 31.8 (1C), 21.8 (1C), 19.1 (1C). HRMS (ESI) calcd for $C_{13}H_{13}N_3O_2S$ $[M+H]^+$ 274.0638, found 274.0646.

2-(benzofuran-2-yl)-7,8-dihydro-5H-pyrido[1,2-a]thiazolo[5,4-d]pyrimidin-10(6H)-one(7ag) Yield 75%, light yellow solid, m p 182–183 °C, HPLC purity: > 98%. ^{1}H NMR (400 MHz, $CDCl_3$) δ 7.68 (d, J = 7.8 Hz, 1H), 7.62 (s, 1H), 7.56 (d, J = 8.3 Hz, 1H), 7.39 (t, J = 7.3 Hz, 1H), 7.30 (t, J = 7.5 Hz, 1H), 4.16 (t, J = 6.1 Hz, 2H), 3.05 (t, J = 6.6 Hz, 2H), 2.34–1.73 (m, 4H). ^{13}C NMR (100 MHz, $CDCl_3$) δ 160.3 (1C), 157.0 (1C), 156.9 (1C), 155.3 (1C), 154.1 (1C), 149.4 (1C), 136.8 (1C), 128.2 (1C), 126.4 (1C), 123.8 (1C), 122.3 (1C), 111.6 (1C), 107.0 (1C), 42.9 (1C), 31.9 (1C), 21.8 (1C), 19.0 (1C). HRMS (ESI) calcd for $C_{17}H_{15}N_3O_2S$ $[M+H]^+$ 324.0796, found 324.0801.

2-(thiophen-3-yl)-7,8-dihydro-5H-pyrido[1,2-a]thiazolo[5,4-d]pyrimidin-10(6H)-one(7ah) Yield 71%, light yellow solid, m p 191–192 °C, HPLC purity: > 98%. ^{1}H NMR (400 MHz, $CDCl_3$) δ 8.13–7.94 (m, 1H), 7.69 (d, J = 5.1 Hz, 1H), 7.40 (dd, J = 5.0, 3.0 Hz, 1H), 4.15 (t, J = 6.1 Hz, 2H), 3.02 (t, J = 6.6 Hz, 2H), 2.06–1.93 (m, 4H). ^{13}C NMR (100 MHz, $CDCl_3$) δ 159.8 (1C), 159.1 (1C), 157.0 (1C), 156.6 (1C), 136.4 (1C), 135.4 (1C), 126.8 (1C), 126.4 (1C), 125.9 (1C), 42.8 (1C), 31.9 (1C), 21.8 (1C), 19.1 (1C). HRMS (ESI) calcd for $C_{13}H_{13}N_3OS_2$ $[M+H]^+$ 290.0411, found 290.0416.

2-(benzo[b]thiophen-2-yl)-7,8-dihydro-5H-pyrido[1,2-a]thiazolo[5,4-d]pyrimidin-10(6H)-one(7ai) Yield 59%, light yellow solid, m p 155–156 °C, HPLC purity: > 98%. ^{1}H NMR (400 MHz, $CDCl_3$) δ 8.12–7.66 (m, 3H), 7.60–7.30 (m, 2H), 4.14 (t, J = 6.1 Hz, 2H), 3.03 (t, J = 6.6 Hz, 2H), 2.25–1.80 (m, 4H). ^{13}C NMR (100 MHz, $CDCl_3$) δ 160.5 (1C), 157.9 (1C), 157.1 (1C), 156.6 (1C), 140.8 (1C), 139.3 (1C), 136.7 (1C), 136.4 (1C), 126.1 (1C), 124.9 (2C), 124.5 (1C), 122.6 (1C), 42.9 (1C), 31.9 (1C), 21.8 (1C), 19.0 (1C). HRMS (ESI) calcd for $C_{17}H_{15}N_3OS_2$ $[M+H]^+$ 340.0567, found 340.0573.

2-([1,1'-biphenyl]-2-yl)-7,8-dihydro-5H-pyrido[1,2-a]thiazolo[5,4-d]pyrimidin-10(6H)-one(7aj) Yield 74%, light yellow solid, m p 197–198 °C, HPLC purity: > 98%. ^{1}H NMR (400 MHz, $CDCl_3$) δ 8.22 (d, J = 7.3 Hz, 1H), 7.47 (dd, J = 15.1, 7.3 Hz, 2H), 7.38–7.29 (m, 6H), 4.11 (t, J = 6.2 Hz, 2H), 2.93 (t, J = 6.5 Hz, 2H), 2.21–1.87 (m, 4H). ^{13}C NMR (100 MHz, $CDCl_3$) δ 163.9 (1C), 161.5 (1C), 157.1 (1C), 156.5 (1C), 141.4 (1C), 139.9 (1C), 135.1 (1C), 134.2 (1C), 132.1 (1C), 130.6 (1C), 130.4 (1C), 130.1 (2C), 128.6 (2C), 128.2 (1C), 127.8 (1C), 42.7 (1C), 31.8 (1C), 21.9 (1C), 19.1 (1C). HRMS (ESI) calcd for $C_{21}H_{19}N_3OS$ $[M+H]^+$ 360.1158, found 360.1165.

2-([1,1'-biphenyl]-4-yl)-7,8-dihydro-5H-pyrido[1,2-a]thiazolo[5,4-d]pyrimidin-10(6H)-one(7ak) Yield 77%, light yellow solid, m p 263–264 °C, HPLC purity: > 98%. ^{1}H NMR (400 MHz, $CDCl_3$) δ 8.14 (d, J = 8.2 Hz, 2H), 7.70 (d, J = 8.3 Hz, 2H), 7.64 (d, J = 7.3 Hz, 2H), 7.47 (t, J = 7.5 Hz, 2H), 7.39 (t, J = 7.5 Hz, 1H), 4.16 (t, J = 6.1 Hz, 2H), 3.04 (t, J = 6.6 Hz, 2H), 2.07–1.93 (m, 4H). ^{13}C NMR (100 MHz, $CDCl_3$) δ 164.0 (1C), 160.2 (1C), 157.0 (1C), 156.7 (1C), 143.7 (1C), 139.9 (1C), 136.8 (1C), 131.9 (1C), 128.9 (2C), 127.9 (1C), 127.7 (2C), 127.5 (2C), 127.1 (2C), 42.8 (1C), 31.9 (1C), 21.8 (1C), 19.1 (1C). HRMS (ESI) calcd for $C_{21}H_{19}N_3OS$ $[M+H]^+$ 360.1156, found 360.1165.

2-(4-phenoxyphenyl)-7,8-dihydro-5H-pyrido[1,2-a]thiazolo[5,4-d]pyrimidin-10(6H)-one(7al) Yield 79%, light yellow solid, m p 193–194 °C, HPLC purity: > 98%. ^{1}H NMR (400 MHz, $CDCl_3$) δ 8.01 (d, J = 8.5 Hz, 2H), 7.37 (t, J = 7.7 Hz, 2H), 7.17 (td, J = 7.6, 1.0 Hz, 1H), 7.10–6.98 (m,

4H), 4.11 (t, J = 6.2 Hz, 2H), 3.00 (t, J = 6.5 Hz, 2H), 2.09–1.88 (m, 4H). ^{13}C NMR(100 MHz, $CDCl_3$) δ 163.7 (1C), 160.2 (1C), 160.1 (1C), 157.0 (1C), 156.6 (1C), 155.9 (1C), 136.7 (1C), 130.0 (2C), 128.9 (2C), 127.9 (1C), 124.2 (1C), 119.8 (2C), 118.3 (2C), 42.8 (1C), 31.9 (1C), 21.8 (1C), 19.1 (1C). HRMS (ESI) calcd for $C_{21}H_{19}N_3O_2S$ $[M+H]^+$ 376.1106, found 376.1114.

2-(naphthalen-2-yl)-7,8-dihydro-5H-pyrido[1,2-a]thiazolo[5,4-d]pyrimidin-10(6H)-one(7am) Yield 67%, light yellow solid, m p 242–243 °C, HPLC purity: > 98%. ^{1}H NMR (400 MHz, $CDCl_3$) δ 8.51 (s, 1H), 8.15 (dd, J = 8.6, 1.5 Hz, 1H), 7.99–7.77 (m, 3H), 7.64–7.39 (m, 2H), 4.12 (t, J = 6.1 Hz, 2H), 2.99 (t, J = 6.6 Hz, 2H), 2.36–1.66 (m, 4H). ^{13}C NMR (100 MHz, $CDCl_3$) δ 164.2 (1C), 160.2 (1C), 156.9 (1C), 156.7 (1C), 136.7 (1C), 134.5 (1C), 132.9 (1C), 130.4 (1C), 128.7 (1C), 128.7 (1C), 127.8 (1C), 127.5 (1C), 127.2 (1C), 126.8 (1C), 124.0 (1C), 42.8 (1C), 31.8 (1C), 21.8 (1C), 19.0 (1C). HRMS (ESI) calcd for $C_{19}H_{17}N_3OS$ $[M+H]^+$ 334.1006, found 334.1009.

2-(dibenzo[b,d]furan-4-yl)-7,8-dihydro-5H-pyrido[1,2-a]thiazolo[5,4-d]pyrimidin-10(6H)-one(7an) Yield 68%, light yellow solid, m p 263–264 °C, HPLC purity: > 98%. ^{1}H NMR (400 MHz, $CDCl_3$) δ 8.57 (dd, J = 7.8, 0.9 Hz, 1H), 8.03 (dd, J = 7.6, 0.9 Hz, 1H), 8.01–7.94 (m, 1H), 7.68 (d, J = 8.2 Hz, 1H), 7.48 (dt, J = 15.5, 7.4 Hz, 2H), 7.38 (t, J = 7.5 Hz, 1H), 4.16 (t, J = 6.1 Hz, 2H), 3.05 (t, J = 6.6 Hz, 2H), 2.29–1.81 (m, 4H). ^{13}C NMR (100 MHz, $CDCl_3$) δ 160.9 (1C), 158.4 (1C), 157.2 (1C), 156.6 (1C), 156.1 (1C), 152.8 (1C), 135.5 (1C), 127.7 (1C), 125.9 (1C), 125.2 (1C), 123.6 (1C), 123.4 (1C), 123.1 (1C), 122.9 (1C), 120.8 (1C), 117.8 (1C), 112.1 (1C), 42.8 (1C), 31.9 (1C), 21.9 (1C), 19.1 (1C). HRMS (ESI) calcd for $C_{21}H_{17}N_3O_2S$ $[M+H]^+$ 374.0952, found 374.0968.

Biological assay methods

AChE and BChE inhibition Assays

AChE and BChE inhibitory activities for the tested compounds were obtained using the method of Ellman et al. [39]. AChE, BChE, 5,5′-dithiobis(2-nitrobenzoic acid) (Ellman's reagent; DTNB), acetylthiocholine iodide (ATCI), and butyrylthiocholine iodide (BTCI) were purchased from Sigma-Aldrich. At least six different concentrations (10^{-5}–10^{-7} M) of each test compound were used to determine the enzyme inhibition activity. In brief, the procedure was: 158 μL of AChE (0.02 unit/mL) or BChE (0.02 unit/mL) and 2 μL of the compounds were incubated at 25 °C for 10 min; next, 20 μL of 5 mM substrate (ATCI or BTCI solution) was added, and the solution further incubated at 37 °C for 10 min; finally, 20 μL of 2.5 mM DTNB was added, and the activity measured at a wavelength of 405 nm using the Spectra MAX 190. The IC_{50} value (the concentration of the compound required for a 50% reduction in cholinesterase activity) was calculated using GraphPad Prism 7. The results are expressed as the mean ± SD of at least three experiments performed in triplicate.

Kinetic study of AChE inhibition assay

Kinetic studies were performed in the same manner as the determination of ChEs inhibition [40], while the substrate (ATCI) was used in concentrations of 0.05, 0.1, 0.25, 0.5, 0.75 and 1 mM. The concentrations of test compounds were set to 0, 2.5, 5 and 10 μM for 7o. The enzymatic reaction was extended to 7 min for AChE before the determination of the absorption. The V_{max} and K_m values for Michaelis−Menten kinetics were obtained by a weighted least squares analysis from the substrate velocity curves using GraphPad Prism 7. In addition, the inhibitor constant (K_i) was calculated by linear regression from the Lineweaver–Burk plot versus the inhibitor concentration.

Cell toxicity assay

Materials Doxorubicin was purchased from BBI Inc. (Shanghai, China). 293T cell lines was obtained from the Chinese Type Culture Collection, CAS (Shanghai, China).

Cell cultures 293 T cells were grown in Dulbecco's modified Eagle's medium (DMEM) with 4.5 g/L glucose and 0.37% sodium bicarbonate (Gibco, Rockville, MD, USA). All cell culture media contained 10% FBS and antibiotic mix (1 × 100 μM penicillin A and 100 μM of streptomycin) and were grown at 37 °C in a humidified incubator (Binder, Germany) containing 95% air/5% CO_2 and were fed every 3–4 days.

Proliferation assays All prepared compounds were dissolved in DMSO in a stock concentration of 10 mM. 293 T cells grown in the logarithmic phase were separately seeded in aliquots of 200 μL in 96-well plates at a density of 5×10^3 cells/well. The cells were grown for 24 h in a humidified incubator (Binder, Germany) at 37 °C with 95% humidity and 5% CO_2. Thereafter, the cells were treated with 1, 10, 25 and 30 μM of compounds with IC_{50} less than 10 μM for 48 h. Then 20 μL MTT (5 mg/mL) was added to each well and the plates were incubated at 37 °C. Four hours later, the supernatant was removed and 200 μL of DMSO were added to each well and the multiwell plates were shaken for 10 min to dissolve the crystals. Absorbance was read at a wavelength of 540 nm using the Spectra MAX 190. The IC_{50} values were calculated with the inhibition rate. Inhibi-

tion rate (OD value of control group-OD experiment group)/(OD value of control group–OD value of blank group) [41].

Molecular docking

The crystal structure of AChE (PDB: 4EY7) was initially obtained from the RCSB-PDB database. The complex was prepared by "Prepare protein" module in Discovery Studio software to add missed sidechains and hydrogens and remove the water molecules. Thereafter, compound 7o was also prepared using a "Prepare ligands" module to protonate at pH 7 ± 0.4 and then minimized by "Minimize ligands" module [42]. Docking studies were conducted using AutoDock 4.2 software; the results were visualized and analyzed using PyMOL.

Molecular dynamics

Gromacs 2022.3 software was used for molecular dynamics simulation. For small molecule preprocessing, Amber Tools 22 is used to add the GAFF force field to small molecules, while Gaussian 16W is used to hydrogenate small molecules and calculate RESP potential. Potential data will be added to the topology file of the molecular dynamics system. The simulation conditions were carried out at a static temperature of 300K and atmospheric pressure (1 Bar). Amber 99sb-ildn was used as force field, water molecules were used as solvent (Tip3p water model), and the total charge of the simulation system was neutralized by adding an appropriate number of Na+ ions. The simulation system adopts the steepest descent method to minimize the energy and then carries out the isothermal isovolumic ensemble (NVT) equilibrium and isothermal isobaric ensemble (NPT) equilibrium for 100,000 steps, respectively, with the coupling constant of 0.1 ps and the duration of 100 ps. Finally, the free molecular dynamics simulation was performed. The process consisted of 50,000,000 steps, the step length was 2 fs, and the total duration was 100 ns. After the simulation was completed, the built-in tool of the software was used to analyze the trajectory, and the root-mean-square variance (RMSD), root-mean-square fluctuation (RMSF) and protein rotation radius of each amino acid trajectory were calculated, combined with the free energy (MMGBSA), free energy topography and other data.

Supplementary Information The online version contains supplementary material available at https://doi.org/10.1007/s11030-024-10920-x.

Acknowledgements This research was sponsored by the Xinjiang Uygur Autonomous Region"Tianchi Talent"lntroduction Program (Grant No. 2024XGYTCYC07), the Natural Science Foundation of Xinjiang Uygur Autonomous Region (Grant No. 2022D01A340, 2022D01A339); West Light Foundation of the Chinese Academy of Sciences (Grant No. 2023-XBQNXZ-009, 2021-JCTD-001); Special Training Program of Natural Science Foundation of Xinjiang Autonomous Region (2022D03018).

Author contributions Y.Z. and .Z.F.C designed the experiments and wrote the manuscript; Z.Y.Y. performed Molecular docking F.X.Y determined the crystal structure of 7am; L.F.N. performed biological assay; C.N. performed Molecular dynamics. All authors reviewed the manuscript.

Funding The Xinjiang Uygur Autonomous Region "Tianchi Talent"lntroduction Program,2024XGYTCYC07,the Natural Science Foundation of Xinjiang Uygur Autonomous Region,2022D01A340 ,2022D01A339,West Light Foundation of the Chinese Academy of Sciences,2023-XBQNXZ-009,Special Training Program of Natural Science Foundation of Xinjiang Autonomous Region,2022D03018

Declarations

Conflict of interest The authors state no conflict of interest.

References

1. Goedert M, Spillantini MG (2006) A century of alzheimer's disease. Science 314:777–781. https://doi.org/10.1126/science.113281
2. Mendiola-Precoma J, Berumen LC, Padilla K, Garcia-Alcocer G (2016) Therapies for prevention and treatment of alzheimer's Disease. BioMed Res Int. https://doi.org/10.1155/2016/2589276
3. Prati F, Bottegoni G, Bolognesi ML, Cavalli A (2018) BACE-1 inhibitors: from recent single-target molecules to multitarget compounds for alzheimer's disease. J Med Chem 61:619–637. https://doi.org/10.1021/acs.jmedchem.7b00393
4. Thompson PA, Wright DE, Counsell CE, Zajicek J (2012) Statistical analysis: trial design and duration in alzheimer's disease clinical trials: a review. Int Psychogeriatr 24:689–697. https://doi.org/10.1017/s1041610211001116
5. Citron M (2004) Strategies for disease modification in alzheimer's disease. Nat Rev Neurosci 5:677–685. https://doi.org/10.1038/nrn1495
6. Citron M (2010) Alzheimer's disease: strategies for disease modification. Nat Rev Drug Discov 9:387–398. https://doi.org/10.1038/nrd2896
7. Isacson O, Seo H, Lin L, Albeck D, Granholm AC (2002) Alzheimer's disease and Down's syndrome: roles of APP, trophic factors and Ach. Trends Neurosci 25:79–84. https://doi.org/10.1016/S0166-2236(02)02037-4
8. Ittner LM, Goetz J (2011) Amyloid-beta and tau-a toxic pas de deux in alzheimer's disease. Nat Rev Neurosci 12:67–72. https://doi.org/10.1038/nrn2967
9. Roberson ED, Scearce-Levie K, Palop JJ, Yan F, Cheng IH, Wu T, Gerstein H, Yu GQ, Mucke L (2007) Reducing endogenous tau ameliorates amyloid beta-induced deficits in an alzheimer's disease mouse model. Science 316:750–754. https://doi.org/10.1126/science.1141736
10. Cheignon C, Tomas M, Bonnefont-Rousselot D, Faller P, Hureau C, Collin F (2018) Oxidative stress and the amyloid beta peptide in alzheimer's disease. Redox Biol 14:450–464. https://doi.org/10.1016/j.redox.2017.10.014
11. Davies P, Maloney AJF (1976) Selective loss of central cholinergic neurons in alzheimer's disease. Lancet 308:1403–1403. https://doi.org/10.1016/S0140-6736(76)91936-X

12. Bartus RT, Dean R, Beer B, Lippa AS (1982) The cholinergic hypothesis of geriatric memory dysfunction. Science 217:408–414. https://doi.org/10.1126/science.7046051
13. Augustinsson KB, Nachmansohn D (1949) Distinction between acetylcholine-esterase and other choline ester-splitting enzymes. Science 110:98–99. https://doi.org/10.1126/science.110.2847.98
14. Ferris SH (2003) Evaluation of memantine for the treatment of alzheimer's disease. Expert Opin Pharmacother 4:2305–2313. https://doi.org/10.1517/14656566.4.12.2305
15. Koehn FE, Carter GT (2005) The evolving role of natural products in drug discovery. Nat Rev Drug Discov 4:206–220. https://doi.org/10.1038/nrd1657
16. Newman DJ, Cragg GM (2007) Natural products as sources of new drugs over the last 25 years. J Nat Prod 70:461–477. https://doi.org/10.1021/np068054v
17. Butler MS (2008) Natural products to drugs: natural product-derived compounds in clinical trials. Nat Prod Rep 25:475–516. https://doi.org/10.1039/B514294F
18. Li WH, Vederas JC (2009) Drug discovery and natural products: end of an era or an endless frontier? Science 325:161–165. https://doi.org/10.1126/science.1168243
19. Ji HF, Li XJ, Zhang HY (2009) Natural products and drug discovery. EMBO Rep 10:194–200. https://doi.org/10.1038/embor.2009.12
20. Breinbauer R, Vetter IR, Waldmann H (2002) From protein domains to drug candidates-natural products as guiding principles in the design and synthesis of compound libraries. Angew Chem Int Ed 41:2878–2890. https://doi.org/10.1002/1521-3773(20020816)41:16%3c2878::aid-anie2878%3e3.0.co;2-b
21. Ertl P, Roggo S, Schuffenhauer A (2007) Natural product-likeness score and its application for prioritization of compound libraries. J Chem Inf Model 48:68–74. https://doi.org/10.1021/ci700286x
22. Horton DA, Bourne GT, Smythe ML (2003) The combinatorial synthesis of bicyclic privileged structures or privileged substructures. Chem Rev 103:893–930. https://doi.org/10.1021/cr020033s
23. Connolly DJ, Cusack D, Osullivan TP, Guiry PJ (2005) Synthesis of quinazolinones and quinazolines. Tetrahedron 61:10153–10202. https://doi.org/10.1016/j.tet.2005.07.010
24. Fitagerald JS, Johns SR, Lamberton JA, Redcliffe AH (1966) 6,7,8,9-Tetrahydropyridoquinazolines, a new class of alkaloids from *Mackinlaya* species (*Araliaceae*). Aust J Chem 19:151–159. https://doi.org/10.1071/CH9660151
25. Huang XF, Dong YH, Wang JH, Ke HM, Song GQ, Xu DF (2020) Novel PDE5 inhibitors derived from rutaecarpine for the treatment of alzheimer's disease. Bioorg Med Chem Lett. https://doi.org/10.1016/j.bmcl.2020.127097
26. Zeng Y, Nie LF, Bozorov K, Ruzi Z, Song B, Zhao JY, Aisa HA (2022) 2-Substituted tricyclic oxazolo[5,4-d]pyrimidine library: design, synthesis and cytotoxicity activity. J Heterocyclic Chemi 59:555–568. https://doi.org/10.1002/jhet.4401
27. Cabon G, Gaucher B, Gegout A, Heulle S, Masquelin T (2004) Novel solution and solid-phase syntheses of heterocyclic systems. Chimia 57:248–254. https://doi.org/10.2533/000942903777679280
28. Wang J, Cai P, Yang XL, Li F, Wu JJ, Kong LY, Wang XB (2017) Novel cinnamamide-dibenzylamine hybrids: potent neurogenic agents with antioxidant, cholinergic, and neuroprotective properties as innovative drugs for alzheimer's disease. Eur J Med Chem 139:68–83. https://doi.org/10.1016/j.ejmech.2017.07.077
29. Li Q, Xing SS, Chen Y, Liao QH, Xiong BC, He SY, Lu WX, Liu Y, Yang HY, Li QH, Feng F, Liu WY, Chen Y, Sun HP (2020) Discovery and biological evaluation of a novel highly potent selective butyrylcholinsterase inhibitor. J Med Chem 63:10030–10044. https://doi.org/10.1021/acs.jmedchem.0c01129
30. Harel M, Schalk I, Ehret-Sabatier L, Bouet F, Goeldner M, Hirth C, Axelsen PH, Silman I, Sussman JL (1993) Quaternary ligand binding to aromatic residues in the active-site gorge of acetylcholinesterase. Proc Natl Acad Sci 90:9031–9035. https://doi.org/10.1073/pnas.90.19.903
31. Hildebrand PW, Rose AS, Tiemann JKS (2019) Bringing molecular dynamics simulation data into view. Trends Biochem Sci 44:902. https://doi.org/10.1016/j.tibs.2019.06.004
32. Rasheed MA, Iqbal MN, Saddick S, Ali I, Khan FS, Kanwal S, Ahmed D, Ibrahim M, Afzal U, Awais M (2021) Identification of lead compounds against Scm (fms10) in *Enterococcus faecium* using computer aided drug designing. Life (Basel) 11:77. https://doi.org/10.3390/life11020077
33. Bozorov K, Zhao JY, Nie LF, Ma HR, Bobakulov K, Hu R, Rustamova N, Huang GZ, Efferth T, Aisa HA (2017) Synthesis and in vitro biological evaluation of novel diaminothiophene scaffolds as antitumor and anti-influenza virus agents. part 2. RSC Adv 7:31417–31427. https://doi.org/10.1039/C7RA04808D
34. Hodges AJ, Matteucci M, Sharpe A, Sun MH, Wang XJ, Tsui VH (2013) Pyrazol-4-yl-heterocyclyl-carboxamide compounds and methods of use. US2013/79321, A1.
35. Zhang C, Zhong B, Yang SM, Pan LK, Yu SW, Li ZJ, Li SC, Su B, Meng XB (2015) Synthesis and biological evaluation of thiabendazole derivatives as anti-angiogenesis and vascular disrupting agents. Bioorgan Med Chem 23:3774–3780. https://doi.org/10.1016/j.bmc.2015.03.085
36. Nie LF, Bozorov K, Huang GZ, Zhao JY, Niu C, Aisa HA (2018) Design, synthesis, and toward a side-ring optimization of tricyclic thieno[2,3-d]pyrimidin-4(3H)-ones and their effect on melanin synthesis in murine B16 cells. Phosphorus Sulfur Silicon Relat Elem 193:656–667. https://doi.org/10.1080/10426507.2018.1487968
37. Sawa M, Moriyama H, Yamada T, Shitashige M, Kawase Y, Uno Y (2013) Novel bicyclic thiazole compounds. US2013/317218, A1.
38. Yao CL, Jiao B, Yang XL, Xu XB, Dang JS, Zhou GJ, Wu ZX, Lv XQ, Zeng Y, Wong WY (2013) Tris(cyclometalated) iridium(III) phosphorescent complexes with 2-phenylthiazole-type ligands: synthesis, photophysical, redox and electrophosphorescent behavior. Eur J Inorg Chem 27:4754–4763. https://doi.org/10.1002/ejic.201300595
39. Lee SY, Zheng XY, Krishnamoorthy J, Savelieff MG, Park HM, Brender JR, Kim HJ, Derrick JS, Kochi DA, Lee HJ (2014) Rational design of a structural framework with potential use to develop chemical reagents that target and modulate multiple facets of alzheimer's disease. JACS 136:299–310. https://doi.org/10.1021/ja409801p
40. Mo J, Chen TK, Yang HY, Guo Y, Li Q, Qiao YT, Lin HZ, Feng F, Liu WY, Chen Y, Liu ZL, Sun HP (2020) Design, synthesis, in vitro and in vivo evaluation of benzylpiperidine-linked 1,3-dimethylbenzimidazolinones as cholinesterase inhibitors against alzheimer's disease. J Enzym Inhib Med Ch 35:330–343. https://doi.org/10.1080/14756366.2019.1699553
41. Ruzi Z, Nie LF, Bozorov K, Zhao JY, Aisa HA (2021) Synthesis and anticancer activity of ethyl 5-aminol-N-substituted-imidazole-4-carboxylate building blocks. Arch Pharm. https://doi.org/10.1002/ardp.202000470
42. Brooks BR, Bruccoleri RE, Olafson BD, States DJ, Swamina S, Karplus M, Charmm M (1983) CHARMM: a program for macromolecular energy. J Comput Chem 4:187–217. https://doi.org/10.1002/jcc.540040211